

Emptying boxes – classifying transient natural ventilation flows

G. R. HUNT† AND C. J. COFFEY

Department of Civil and Environmental Engineering, Imperial College London, London SW7 2AZ, UK

(Received 8 December 2008; revised 22 October 2009; accepted 23 October 2009)

The buoyancy-driven flushing of fluid from a rectangular box via connections in the base and top into quiescent surroundings of uniform density is examined. Our focus is on the transient flows that develop when the interior is either initially stably stratified in two homogeneous layers – a dense layer below a layer at ambient density, or is filled entirely with dense fluid. Experiments with saline stratifications show that four distinct patterns of flow are possible. We classify these patterns in terms of the direction of flow through the base opening and the propensity of replacement fluid through the top opening to induce interfacial mixing. Unidirectional or bidirectional flow through the base opening may occur and within these two flow types either weak or vigorous interfacial mixing. We identify the three controlling geometrical parameters that determine which flow pattern is established, namely the fractional initial layer depths, the relative areas of the top and base openings and the horizontal length scale of the top opening relative to the initial dense layer depth. We show that these parameters may be reduced to two Froude numbers – one based on the fluxes through the base opening and whose value sets the direction of flow, and a second based on conditions at the top opening whose value determines the vigour of interfacial mixing. Theoretical models are developed for predicting the conditions for transition between each flow pattern and expressed as critical values of the Froude numbers identified.

1. Introduction

In the seventeenth century, Evangelista Torricelli considered the draining of liquids under gravity from a vessel through small openings. He examined the case where the density difference ($\Delta\rho$) between the draining fluid and the ambient environment was large, focusing on water draining in air. Torricelli's law gives the speed of the liquid at the opening as $v = \sqrt{2gh}$ (Torricelli 1643; Batchelor 1967), where g is the acceleration due to gravity, and h the vertical distance between the free surface and the centre of the opening. We revisit this basic problem (hereafter the 'emptying box') but instead focus on the Boussinesq case where the density difference between the draining fluid and ambient environment is small compared with a reference density. Mixing between the two fluids then plays a role both in its influence on the rate of draining and on the developing stratification within the body of the draining fluid. The basic situation considered is shown in figure 1.

The draining of a fluid from a container (a box), initially *filled* with fluid slightly denser than the quiescent ambient, via base openings only and via a combination

† Email address for correspondence: gary.hunt@imperial.ac.uk

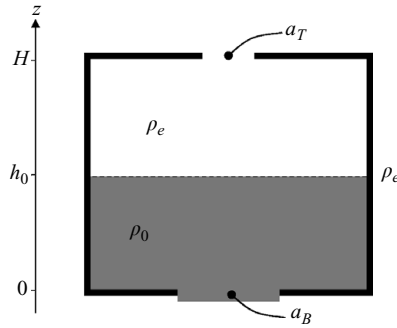


FIGURE 1. Schematic showing the situation considered herein.

of base and top openings, has been examined by Linden, Lane-Serff & Smeed (1990). Their experiments, in which saline solutions were drained from containers into still fresh water environments, showed that horizontal openings positioned at a single (low) level enabled an exchange flow in which vigorous turbulent mixing was observed between inflowing plumes at ambient density and the denser interior. A slow dilution of the interior, which remained at an approximately uniform density, resulted. These flows are often referred to as ‘mixing flows’. Epstein (1988) considered the buoyancy-driven exchange of fluid across circular openings, of diameter d_B in a horizontal boundary of thickness l_B , and showed that the dimensionless volume flux through these openings is of the form $Q/\sqrt{d_B^5 g'} = f(l_B/d_B)$, where $g'(t) = g\Delta\rho(t)/\rho_e$ is the reduced gravity at a time t , $\Delta\rho$ the density step across the opening and ρ_e a reference density. For $l_B/d_B \ll 1$, experiments by Epstein (1988) supported the scaling $Q/\sqrt{d_B^5 g'} = k \approx 0.055$. By assuming that a uniform density profile is maintained in the box, which requires that the incoming fluid mixes instantaneously and completely throughout the interior, Linden *et al.* (1990) used Epstein’s result to show that the interior density tends algebraically to the exterior density on a time scale τ :

$$\frac{\Delta\rho(t)}{\Delta\rho_0} = \frac{g'(t)}{g'_0} = \left(1 + \frac{t}{\tau}\right)^{-2}, \quad \tau = \frac{2V}{ka_B(g'_0 d_B)^{1/2}}, \quad (1.1)$$

where V is the volume of the box and a_B the area of the base opening. In (1.1), $g'_0 = g\Delta\rho_0/\rho_e$ is the initial reduced gravity of the interior, achieved with an initial density contrast $\Delta\rho_0$.

In order to distinguish between flows we identify in §3 for which there is vigorous but not complete mixing, we refer to mixing flows in which the interior remains at (approximately) uniform density for all time as ‘classical mixing flows’. In our experiments (§3) a non-uniform stratification evolved in the interior when one or more base openings were positioned at a single level. For this reason we refer to flows for which bidirectional flow occurs through the base opening(s) as ‘exchange flows’ and distinguish between the dynamics at the level of the opening and the developing stratification.

Experiments by Linden *et al.* (1990) also showed that openings both in the base and top of a box (of areas a_B and a_T , respectively) can result in an efficient means of flushing the interior. They refer to the resulting flow as ‘displacement flow’ as dense fluid drains out through the base opening(s) and is replaced, in the absence of

mixing, by fluid at ambient density drawn in through the top opening(s). In contrast to mixing flow there is unidirectional flow through each opening. Linden *et al.* (1990) characterize the combination of top and base openings using an ‘effective’ opening area, which Hunt & Linden (2001) express as

$$A^* = \left(\frac{1}{2c_T^2 a_T^2} + \frac{1}{2c_B^2 a_B^2} \right)^{-1/2}, \quad (1.2)$$

where c_T and c_B are loss coefficients (normally assumed constant for high-Reynolds-number flow) for the top and base openings, respectively. They observed that interfacial mixing due to the inflow was negligible and that a two-layer stratification and ‘displacement flow’ was established and maintained throughout the transients. Linden *et al.* (1990) report on flows established with top opening areas greater than twice the base opening areas ($a_T > 2a_B$) and that, with this geometry, evidence of weak mixing induced by the inflow is visible inside their box (Linden *et al.* 1990, figure 8). We return to these results in §4.1 and §5 in the context of our full classification of emptying-box flows.

Linden *et al.* (1990) determined the dependence of the rate of flushing for displacement flows $Q(t) \equiv Q_d(t)$ on the density contrast $\Delta\rho(t)$ (assumed constant and equal to $\Delta\rho_0$ due to the absence of buoyancy transfers between fluid and box) and instantaneous saline layer depth. Assuming no mixing between the inflowing ambient fluid and the interior they showed

$$Q_d(t) = A^* \left[\int_0^H g' dz \right]^{1/2} = A^* \sqrt{g_0' h(t)} \quad (1.3)$$

and that the layer depth is well described by

$$\frac{h(t)}{H} = \left(1 - \frac{t}{t_E} \right)^2, \quad t_E = \frac{2S}{A^*} \left(\frac{H}{g_0'} \right)^{1/2}, \quad (1.4)$$

where t_E is the time taken for dense fluid of initial depth H to empty completely from a box of cross-sectional area S (independent of height) via openings of effective area A^* . Hereafter, we refer to displacement flow in the absence of mixing as ‘classical displacement flow’.

Mixing and displacement flows are regarded as the two basic modes of flushing. Their relative flushing rates are considered in detail by Coffey & Hunt (2007) in the context of ventilation effectiveness where it is shown that mixing flow may provide the most effective means of flushing, at least for a portion of the draining period. In the context of a ventilated room or the flushing of a gaseous pollutant following an accident, it may be desirable to establish a combination of the two basic modes of flushing (see §3), i.e. to locally induce mixing whilst achieving a bulk displacement of fluid from the room.

In this paper we revisit the basic problem of flushing dense fluid from a box, via openings in the top and base, into quiescent surroundings of uniform density (figure 1). The interior is initially filled, or partially filled, with fluid of uniform density ρ_0 so that, in general, the initial stratification is in two homogeneous layers – a dense layer below a layer at ambient density. We restrict our attention to density differences between the dense fluid and the ambient that are small compared with the ambient density so that the Boussinesq approximation is valid. We examine this ‘emptying box’ through a series of laboratory experiments and present complementary theoretical models for predicting the transition between the different patterns of flow we identify.

Our aim is to examine how the stratification, flow patterns and flushing times depend on the initial stratification and the geometry of the box (e.g. the ratio $R = a_T/a_B$ of top and base opening areas). Our observations and measurements show that the classical displacement and classical mixing flows previously identified represent only a subset of the possible flow patterns that can be established. Furthermore, we demonstrate that these classical flows occur within only a relatively small region of the overall parameter space – when there is either no mixing or there is complete mixing, respectively, between inflowing replacement fluid and interior fluid. Thus, these classical flows may be regarded as limiting cases, or indeed idealized cases, in terms of the extent of mixing and direction of flow they induce.

We show that, in general, the inflow of ambient replacement fluid required for volume conservation mixes with the denser interior fluid and that, consequently, the developing stratification and flushing times are not well predicted by current displacement-flow or mixing-flow theories. Relatively small departures from area ratios and initial stratifications that result in a classical displacement flow are shown to result in significant interfacial mixing and the formation of an intermediate layer which deepens to *fill*, rather than being flushed from, the box. Further departures give rise to bidirectional flow at the base with the associated turbulent mixing, albeit of insufficient vigour to give rise to the (approximately) uniform density environment synonymous with classical mixing flow. In contrast, one may observe a combination of both turbulent mixing, confined to the interface region, driven by flow through the top and further turbulent dilution of the interior fluid due to bidirectional flow through the base.

The paper is structured as follows. The experimental apparatus is described in §2. The results of our experiments are reported in §3. These results highlight for the first time the range of flow patterns that may be established in emptying boxes with base and top openings. We then provide a classification for the different flows observed and describe the transitions between them. In §4, we develop theoretical models to predict the conditions that give rise to these transitions and compare predictions with our classification deduced from experiments. Finally, our conclusions are drawn in §5.

2. Experiments

A glass-sided visualization tank (of internal horizontal cross-section 250 cm × 125 cm) was filled to a depth of 125 cm with fresh water. Inside, a clear rectangular Perspex box (wall thickness 1 cm) with internal dimensions $H = 30$ cm and $S = 30 \times 40$ cm was suspended rigidly approximately 20 cm below the free surface. A number of circular holes (diameters 3 cm and 5 cm) in the top and base horizontal faces of the box provided connections between the box interior and the quiescent exterior. These holes could be plugged using Perspex disks with integral rubber O-rings to provide a water-tight seal. The hole sizes, numbers and locations allowed opening areas to be considered within the ranges $0 \leq a_T \leq 242.0$ (cm²) and $7.1 \leq a_B \leq 39.2$ (cm²). The water in the tank and a saline solution in a separate 140 litre container were allowed to stand for a number of hours and warm to room temperature prior to beginning an experiment.

The base holes of the flooded box were initially plugged and the top holes opened. A two-layer stratification was then set up – a saline layer of uniform density ρ_0 and depth h_0 below a fresh water layer of density ρ_e . A sample was extracted from the uniform lower layer and the density measured with an Anton Paar DMA 35N density

meter (accuracy $\pm 0.001 \text{ g cm}^{-3}$). The initial stratification was thus characterized by the pair $\{\xi_0, g'_0\}$, where $\xi_0 = h_0/H$ denotes the fractional initial saline layer depth and $g'_0 = g(\rho_0 - \rho_e)/\rho_e$ the initial reduced gravity of the saline layer.

Openings in the top of the box were then plugged until the required value of a_T was obtained with one, or more, openings. At time $t = 0$, one or more plugs were removed from the base of the box to give the desired value of a_B and start the experiment. Where possible single openings were used in the top and/or base. When this was not possible due to the box design, following Linden *et al.* (1990), a_T and a_B were taken to be equal to the sum of the areas of the openings in the top and base, respectively. These total areas were recorded and used in the analysis.

The apparatus was lit using either collimated light from an Elmo 253E slide projector and the flow visualized using a shadowgraph, or diffusively backlit with a bank of high-frequency fluorescent tubes and the flow visualized by initially staining the lower layer uniformly with methylene blue. Shadowgraph images (figures 4, 6, 8, 10 and 14) were enhanced by correcting for the background variation in the lighting. Experiments were recorded using a CCD camera (a JAI CV-M4+CL, resolution $1392(\text{h}) \times 1040(\text{v})$) connected to a frame grabber and the captured digital images analysed using the DigiFlow software (Dalziel 1993). A dye-attenuation technique (Hacker, Linden & Dalziel 1996 and Cenedese & Dalziel 1998) and camera fitted with a red filter (Hoya R(25A)) were used in a subset of experiments to obtain non-intrusive and synoptic measurements of the horizontally averaged density stratification. Density profiles were deduced by width-averaging (left-to-right in figure 4) across a window extending from the base to the top of the box – the window location was chosen to avoid any localized turbulent regions where the assumption of horizontal homogeneity breaks down. Densities inferred using this technique were typically within 5% of those measured directly using the density meter. Due to the optical nature of the dye-attenuation technique, measurements made within approximately 3 cm of the base proved unreliable due to reflections. Buoyancy frequency profiles (figures 5, 7, 9, 11 and 12) were calculated from the measured density profiles using a five-point central-differencing method. Determination of whether the flow was unidirectional or bidirectional was made by eye – a time-varying lower layer density was also evidence of bidirectional flow. The initial fractional layer depths and initial reduced gravities considered were in the ranges $0.1 \leq \xi_0 \leq 1$ and $15 \leq g'_0 \leq 100 \text{ (cm s}^{-2}\text{)}$, respectively. In total over 250 separate experiments were performed.

3. Flow regimes

We restrict our attention to high-Reynolds-number and high-Péclet-number flows (typically $Re = O(10^4)$, $Pe = O(10^6)$) so that viscous effects are negligible and advection dominates the effects of molecular diffusion. Furthermore, we assume in our theoretical developments (§4) that there are no transfers of buoyancy between the fluid and the box boundaries, as is the case in our experiments. Additionally, we consider box geometries for which $\{a_T, a_B\} \ll S$. Specifically, for our experiments $0 \leq a_T/S \lesssim 0.2$ and $0.006 \lesssim a_B/S \lesssim 0.03$. Pressures within the box are thus expected to vary approximately hydrostatically as assumed in our model of the transitions between the flows we identify (§4).

3.1. Dimensional considerations

Linden *et al.* (1990) scale the emptying-box problem using the vertical distance between the openings (H) as the primary length scale – this scale being equal to their

initial saline layer depth. For the two-layer initial stratification we consider, the initial layer depth h_0 provides the most appropriate scaling as this scale determines the initial driving buoyancy force. Thus, we denote $\hat{z} = z/h_0$ as the dimensionless vertical coordinate, with origin $\hat{z} = 0$ coincident with the (internal) base of the box (figure 1), $\hat{t} = t\sqrt{g'_0/h_0}$ as dimensionless time and express the dimensionless reduced gravity in the box $\hat{g}' = g'(z, t)/g'_0$ by the functional form

$$\hat{g}' = \hat{g}' \left(\frac{a_T}{h_0^2}, \frac{a_B}{h_0^2}, \frac{H}{h_0}, \frac{z}{h_0}, t\sqrt{\frac{g'_0}{h_0}} \right). \quad (3.1)$$

By considering the limiting cases of classical displacement and classical mixing flows, we expect the relative areas of the openings (i.e. $R = a_T/a_B$) to be physically significant; in these limits $R \rightarrow \infty$ and $R = 0$, respectively. Therefore, for convenience and to aid physical interpretation, we rewrite the governing dimensionless parameters and express \hat{g}' in the form $\hat{g}' = \hat{g}'(R, \xi_0, \lambda_T, \hat{z}, \hat{t})$ where

$$R = \frac{a_T h_0^2}{h_0^2 a_B} = \frac{a_T}{a_B}, \quad \xi_0 = \left(\frac{H}{h_0} \right)^{-1} = \frac{h_0}{H} \quad \text{and} \quad \lambda_T = \left(\frac{a_T}{h_0^2} \right)^{1/2} = \frac{\sqrt{a_T}}{h_0}. \quad (3.2)$$

The three geometric parameters (3.2) are, thus, the ratio R of the top and base opening areas, the fractional initial dense layer depth ξ_0 and a measure λ_T of the length scale characterizing the top opening area relative to the initial dense layer depth. For a circular opening of radius $r_T = \sqrt{a_T/\pi}$, $\lambda_T = \pi^{1/2} r_T/h_0 = \pi^{1/2} r_T g'_0/w_T^2$ where the velocity $w_T = \sqrt{h_0 g'_0}$. Thus, λ_T is a Richardson number relating an initial buoyancy-induced velocity based on the scale of the opening to the initial velocity through the opening. Hence λ_T may be expected to characterize turbulent mixing due to the inflow of replacement fluid through the top when the flow is controlled by the top opening (see §4.1). We could have alternatively formed the parameter $\lambda_B = \sqrt{a_B}/h_0$ ($\equiv \lambda_T/\sqrt{R}$) which may be expected to characterize the flow when it is controlled by the base opening (see §4.2). However, we shall see in §4 that λ_T (or λ_B) alone is not sufficient to fully characterize these flows, and that two distinct Froude numbers $Fr_T(R, \lambda_T, \xi_0)$ and $Fr_B(R, \lambda_B, \xi_0)$ are required.

Linden *et al.* (1990) worked with the single dimensionless parameter A^*/H^2 and showed it was sufficient to characterize displacement flows in the absence of mixing; we show herein that the individual parameters $\{R, \xi_0, \lambda_T\}$, which A^*/H^2 may be expressed in terms of, i.e.

$$\frac{A^*}{H^2} = 2^{1/2} \left(\frac{h_0}{H} \right)^2 \frac{a_T a_B}{h_0^2 a_T} \left(\frac{1}{c_B^2} + \frac{1}{c_T^2} \left(\frac{a_B}{a_T} \right)^2 \right)^{-1/2} = 2^{1/2} \frac{\xi_0^2 \lambda_T^2}{R} \left(\frac{1}{c_B^2} + \frac{1}{c_T^2 R^2} \right)^{-1/2}, \quad (3.3)$$

are necessary to characterize general emptying-box flows.

The effect of the individual parameters (3.2) on flow in an emptying box has not previously been considered. Previous work on displacement flow characterizes the transient behaviour in terms of the effective opening area and without reference to the area ratio R or length scale ratio λ_T . Whilst previous models would suggest that displacement flow is established for any given opening geometry with $\{a_T, a_B\} > 0$, we show that this is not the case and that there is only a limited range of $\{R, \xi_0, \lambda_T\}$ parameter space for which displacement flow is realized.

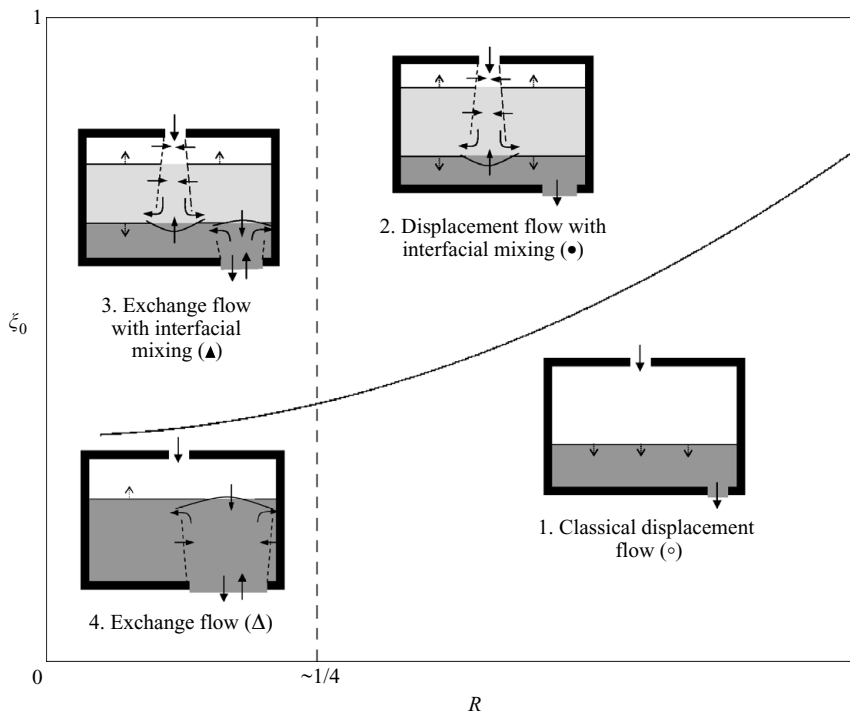


FIGURE 2. Flow regime diagram 1. A slice, for constant λ_T , through $\{R, \xi_0, \lambda_T\}$ space showing schematics of the four flow patterns observed. Solid arrows indicate the direction of flow and dotted arrows the direction of motion of density interfaces. The symbol (\circ , \bullet , \blacktriangle or Δ) accompanying each schematic matches with figure 3. The dashed line indicates the boundary between regimes (1 and 2) in which the flow was unidirectional and regimes (3 and 4) in which the flow through the base was bidirectional. The solid line indicates the boundary between regimes (2 and 3) where interfacial mixing resulted in the formation of an intermediate layer, and regimes (1 and 4) where two layers persisted.

3.2. Observations

Four qualitatively distinct flow patterns were observed depending on R , ξ_0 and λ_T that gave a bulk vertical flow through the box. Consistent with the dimensional considerations (§ 3.1), the initial reduced gravity, g'_0 , only affected the time scales of the draining and not the flow pattern attained for a given $\{R, \xi_0, \lambda_T\}$. Figures 2 and 3, hereafter the ‘Flow Regime Diagrams’, indicate the flow pattern observed for a given $\{R, \xi_0, \lambda_T\}$. Figure 2 shows schematically the main features of the flow patterns identified and figure 3 illustrates the groupings of these flow patterns based on our experimental observations. Each individual experiment performed is marked as a symbol in figure 3 and the four different symbols (\circ , \bullet , \blacktriangle , Δ) correspond to the distinct flow patterns observed – the grouping of these symbols indicates that the parameter space may be divided into four regions. A fifth pattern exists when $a_B = 0$, however, transport of fluid from the box is then solely by molecular diffusion for $a_T > 0$ and this limit will not be discussed further. The solid line in figure 3 shows the line of constant Froude number $Fr_T(0) = 0.67$ (see § 4.1). The dashed line shows $Fr_B(0) = 0.33$ (see § 4.2). These lines mark our theoretical predictions of the flow pattern transitions.

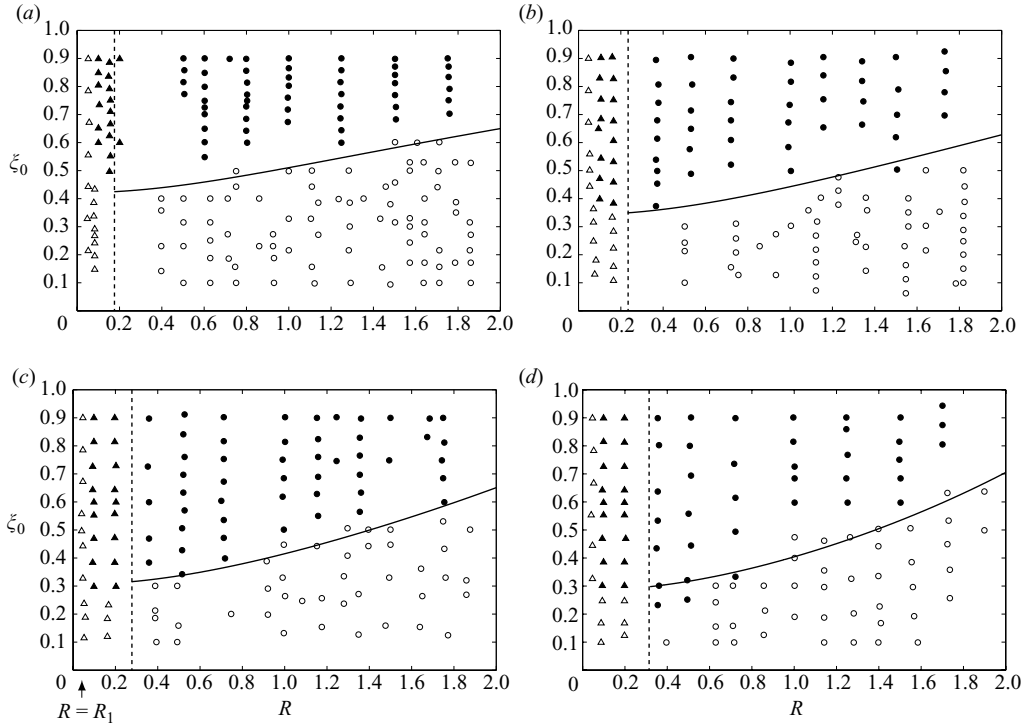


FIGURE 3. Flow regime diagram 2. ξ_0 versus R for $\lambda_T = 0.1$ (a), 0.2 (b), 0.3 (c) and 0.4 (d). For $R \gtrsim 1/4$ unidirectional flows were observed (\circ and \bullet). For $R \lesssim 1/4$ bidirectional flow was observed at the base (Δ and \blacktriangle). The hollow symbols (\circ , Δ) mark flow patterns 1 and 4, respectively, and indicate values of $\{R, \xi_0, \lambda_T\}$ for which mixing was weak between the high-level inflow and the denser interior fluid. The solid symbols (\bullet , \blacktriangle) mark flow patterns 2 and 3, respectively, and indicate values of $\{R, \xi_0, \lambda_T\}$ for which vigorous mixing was observed between the high-level inflow and the denser interior fluid. The solid line shows $Fr_T(0) = 0.67$ and the dashed line $Fr_B(0) = 0.33$ as deduced from our theoretical arguments (§4).

For sufficiently large values of R ($\gtrsim 1/4$ in our experiments), unidirectional flows (\circ , \bullet) were observed through the top and base openings – fluid at ambient density entered the box through the top and dense fluid drained out through the base. Initial conditions/box geometries giving rise to classical displacement flow are shown by hollow circles (\circ) in figure 3. We note that this flow occurs for only a subset of $\{R, \xi_0, \lambda_T\}$. As R decreased, a classical displacement flow could only be maintained by decreasing the initial layer depth ξ_0 ; the decrease in ξ_0 required became more significant as λ_T increased – compare figures 3(a) and 3(d).

For sufficiently small R ($\lesssim 1/4$), bidirectional flows (Δ , \blacktriangle) were established at the base whilst the flow of replacement fluid through the top remained a unidirectional inflow. The flows observed at the values of $\{R, \xi_0, \lambda_T\}$ given by the hollow triangles (Δ) were visually similar below the level of the interface to the classical mixing flow identified by Linden *et al.* (1990). The bulk of the fluid exchange, in to and out of the box, occurred at the base opening but with the associated vigorous mixing between the saline layer and inflowing fluid at ambient density confined to within the lower dense layer. For $R \lesssim R_1$ ($R_1 \approx 0.05$, figure 3), this mixing flow was maintained for all layer depths examined ($0.1 \leq \xi_0 \leq 1$).

a_T (cm ²)	a_B (cm ²)	h_0 (cm)	g'_0 (cm s ⁻²)	t_E (s)	R	λ_T	ξ_0	Flow pattern observed	$Fr_T(0)$	$Fr_B(0)$
59.1	7.1	20.1	31.8	319.0	8.32	0.38	0.67	1 (figures 4, 5)	0.14	2.32
7.1	19.6	18.6	24.8	366.9	0.36	0.14	0.62	2 (figures 6, 7)	1.16	0.60
3.1	19.6	20.1	35.1	699.0	0.16	0.09	0.67	3 (figures 8, 9, 13)	1.18†	0.28
0.2	19.6	21.0	22.0	13817.7	0.01	0.02	0.70	4 (figures 10, 11)	0.46‡	0.02

TABLE 1. Geometry and initial conditions for the experiments presented in figures 4–13. $Fr_T(0)$ and $Fr_B(0)$ were evaluated using (4.4) and (4.13), respectively. †Entries of $Fr_T(0)$ for bidirectional flows are inaccurate as $Fr_T(0)$ is developed assuming unidirectional flow, however, for flow pattern 3 the error in the estimate of $Fr_T(0)$ is expected to be small due to weak exchange at the base. ‡For flow pattern 4 the exchange is vigorous and the estimate of $Fr_T(0)$ is expected to be unreliable.

The solid symbols (●, ▲) on the flow regime diagrams indicate the region of $\{R, \xi_0, \lambda_T\}$ space for which vigorous mixing on the interface driven from above, by replacement fluid through the top, was observed (the hollow symbols (○, △) indicate the regions of $\{R, \xi_0, \lambda_T\}$ parameter space for which the high-level inflow did not result in vigorous mixing). In these experiments an intermediate layer formed and deepened to eventually fill the box. The extent of the mixing was assessed by examining the evolution of horizontally averaged buoyancy frequency profiles; if two peaks were maintained this was an indication that two density interfaces were present/persisted and, thus, that an intermediate layer had formed. Under these conditions the mixing is referred to as ‘vigorous’.

One may also designate an additional flow pattern for the small region of the parameter space where $\xi_0 \ll 1$. For the four flow patterns considered herein, the bulk of the flow within the box is in the vertical direction. However, if the initial layer of dense fluid is sufficiently thin, then the flow realized is fundamentally different – the bulk flow within the layer is in the horizontal direction. Work on this thin-layer case is currently being addressed for a future paper and yields the possibility of non-selective withdrawal (Turner 1973).

In the following sections (§§ 3.3 and 3.4) we present shadowgraph images, reduced gravity profiles and buoyancy frequency profiles to assist in our description of and to highlight the differences between the four flow patterns. The conditions for the experiments described are listed in table 1. Images are shown at various times throughout the transients. Time has been scaled on the ‘emptying time’ t_E (from (1.4) with H replaced with h_0 and $c_B = c_T = 0.6$ in A^* (1.2)) rather than on $\sqrt{h_0/g'_0}$; the former scaling allows each flow to be compared directly with the no-mixing classical displacement flow limit in which the box empties completely of dense fluid in a time $t/t_E = 1$. Dimensionless times given are rounded to two decimal places.

3.3. Unidirectional flows

For $R \gtrsim 1/4$, the flow through both the top and base was unidirectional for the entire range of ξ_0 and λ_T examined (figure 3). Replacement fluid at ambient density entered solely through the top and dense fluid drained out through the base.

3.3.1. ○ Pattern 1. Classical displacement flow

Figure 4 depicts the flushing of dense fluid from the box by classical displacement flow. These shadowgraph images were recorded from a typical experiment falling in the region of $\{R, \xi_0, \lambda_T\}$ space indicated by the hollow circles (○) in the flow

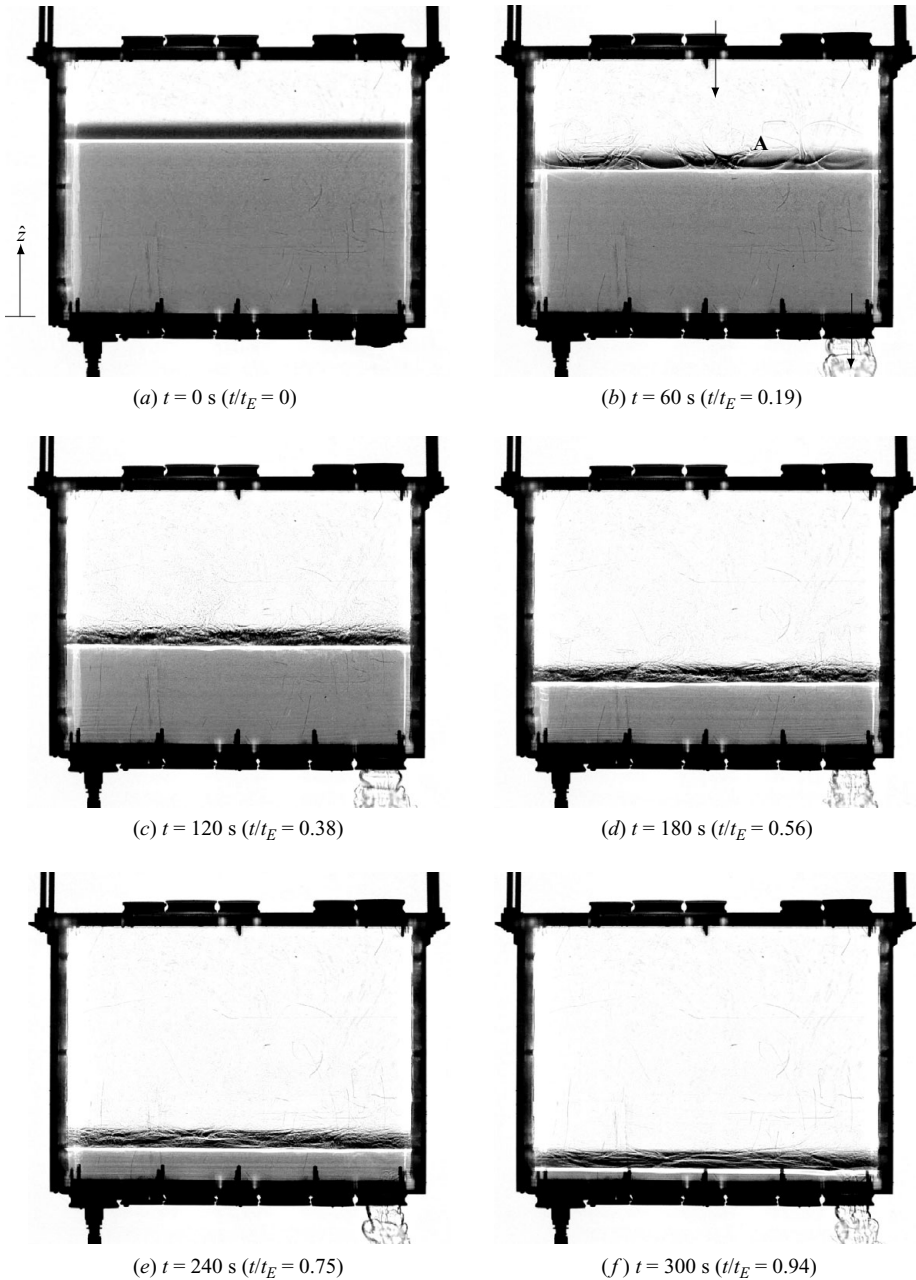


FIGURE 4. The unidirectional flow pattern ‘classical displacement flow’ (○ in the flow regime diagrams). The arrows in (b) indicate the direction of flow maintained through the openings. (a) The initial stratification. (b)–(f) Images show the basic two-layer stratification is maintained.

regime diagrams. Corresponding dimensionless reduced gravity ($\hat{g}'(\hat{z})$) and buoyancy frequency ($N^2(\hat{z}) = \partial \hat{g}' / \partial \hat{z}$) profiles are shown in figure 5. Whilst this flow pattern is described by Linden *et al.* (1990), figures 4 and 5 are included here to allow direct comparisons with the other flow patterns we identify.

The rate at which the dense fluid drained out decreased as was evident by both the decreasing rate of descent of the interface and by transition in the plume flowing from

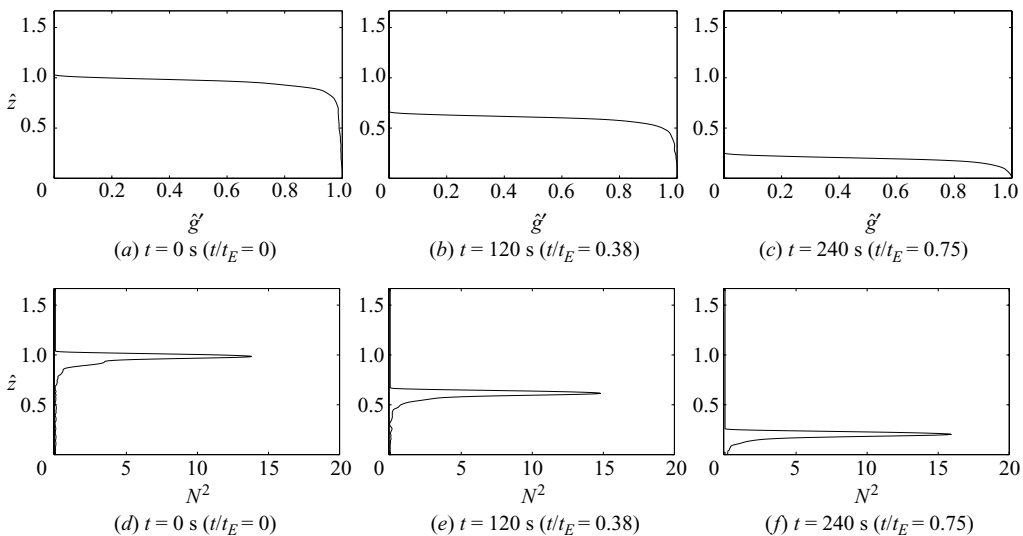


FIGURE 5. Reduced gravity profiles $\hat{g}'(\hat{z}) = g'(\hat{z})/g'_0$ in (a)–(c) and buoyancy frequency profiles $N^2(\hat{z}) = \partial\hat{g}'(\hat{z})/\partial\hat{z}$ in (d)–(f) of the ‘classical displacement flow’ experiment shown in figure 4.

the base opening into the ambient – from, in general, an initially highly turbulent forced flow (Morton 1959) to one in which regular vortex generation immediately downstream of the source was observed. The descending interface between the dense and ambient layers either remained undisturbed or developed smooth cup-like indentations resulting from impingement by the jet-like inflow. Slight scouring was observed in the form of wisps of fluid being lifted from the interface (region denoted **A** in figure 4*b*), however, there was no discernable increase of the upper layer density and the basic two-layer stratification was maintained (figure 4*b–f*). Evidence of the persisting two layers can also be seen in the profiles of figure 5. Apart from a vertical displacement, the shape of the reduced gravity profiles remains almost constant. As expected for classical displacement flow, there is a single peak in the buoyancy frequency profile; the characteristics of which remain constant over time which, in accord with the reduced gravity profiles, indicates that negligible mixing and diffusion have taken place over the time scale of the draining. Disturbances on the density interface were observed to increase as the top opening area was decreased relative to the base opening area, i.e. as R decreased. Nevertheless, entrainment of dense fluid into the ambient layer, as a result of replacement fluid impinging on the interface, was weak and only visible as fine tendrils of fluid rising from the dense layer below, with no measurable increase in the upper layer density.

3.3.2. ● Pattern 2. Displacement flow with interfacial mixing

Disturbances on the interface driven by inflow through the top of the box continued to increase as R decreased (e.g. on increasing a_B for a fixed $\{\xi_0, \lambda_T\}$), or as ξ_0 was increased on increasing h_0 (for a fixed $\{R, \lambda_T\}$), until eventually the inflow was highly turbulent and sufficiently energetic to drive vigorous mixing at the interface. The solid circles (●) in the flow regime diagrams indicate unidirectional flow but where the structure of the stratification departed from the initial two layers due to the inflow penetrating the interface. The basic structure of the stratification then changed from two- to three-layer owing to a flux of buoyancy from the dense layer at the region of impingement. We refer to this flow as ‘displacement flow with interfacial mixing’.

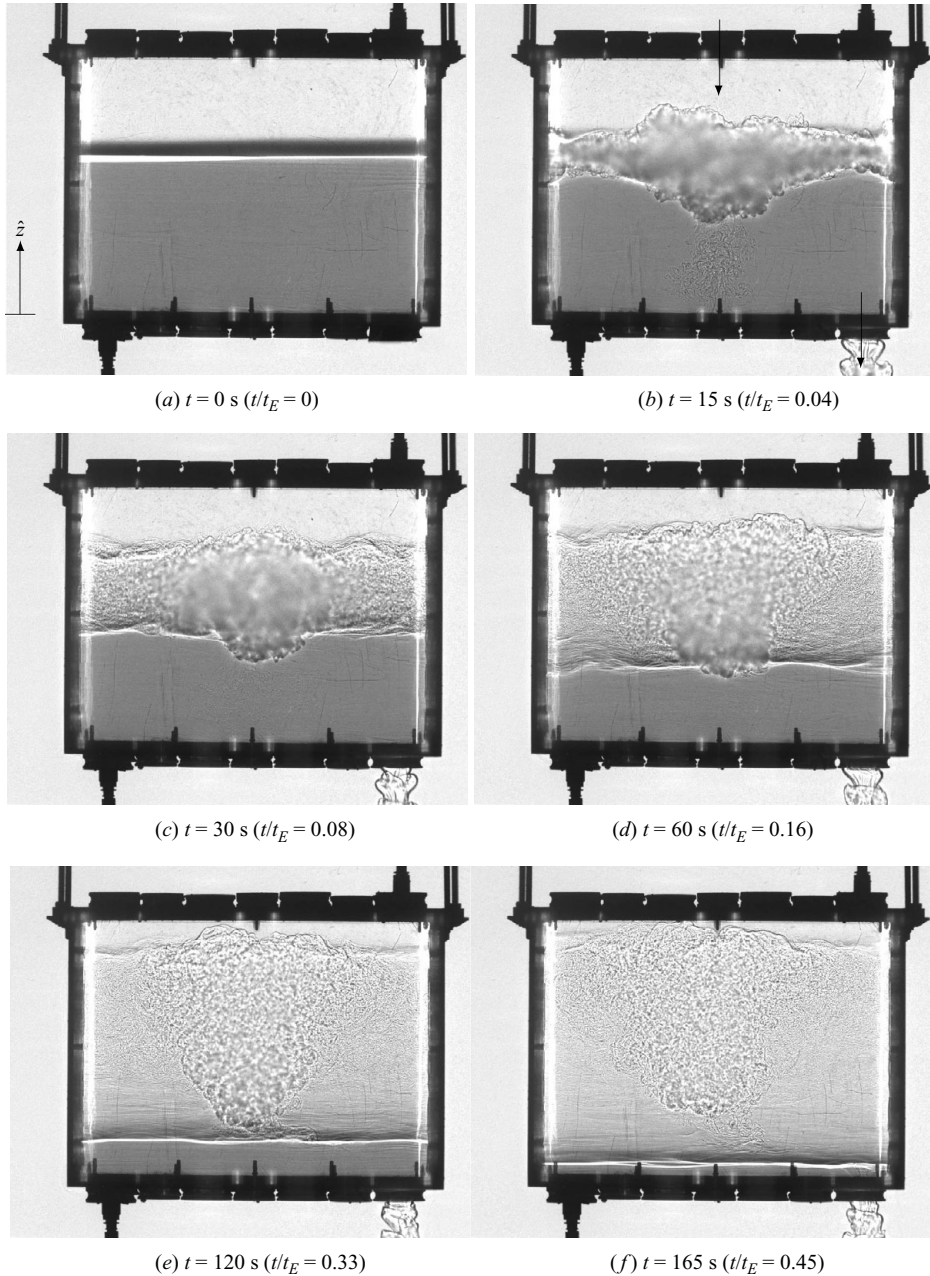


FIGURE 6. The unidirectional flow pattern ‘displacement flow with interfacial mixing’ (● in the flow regime diagrams). The arrows in (b) indicate the direction of flow maintained through the openings. (a) The initial stratification. (b)–(f) Vigorous mixing, due to the inflowing ambient fluid, is visible at the interface and results in the formation of an intermediate layer which deepens. In (e) and (f) the fountain driven by the inflow in the intermediate layer collapses prior to reaching the lower interface.

Figure 6 depicts the typical draining observed. The vigorous mixing driven by the inflow and the three-layer stratification that developed and persisted can clearly be seen on the shadowgraph. During the initial development the inflowing jet impinged

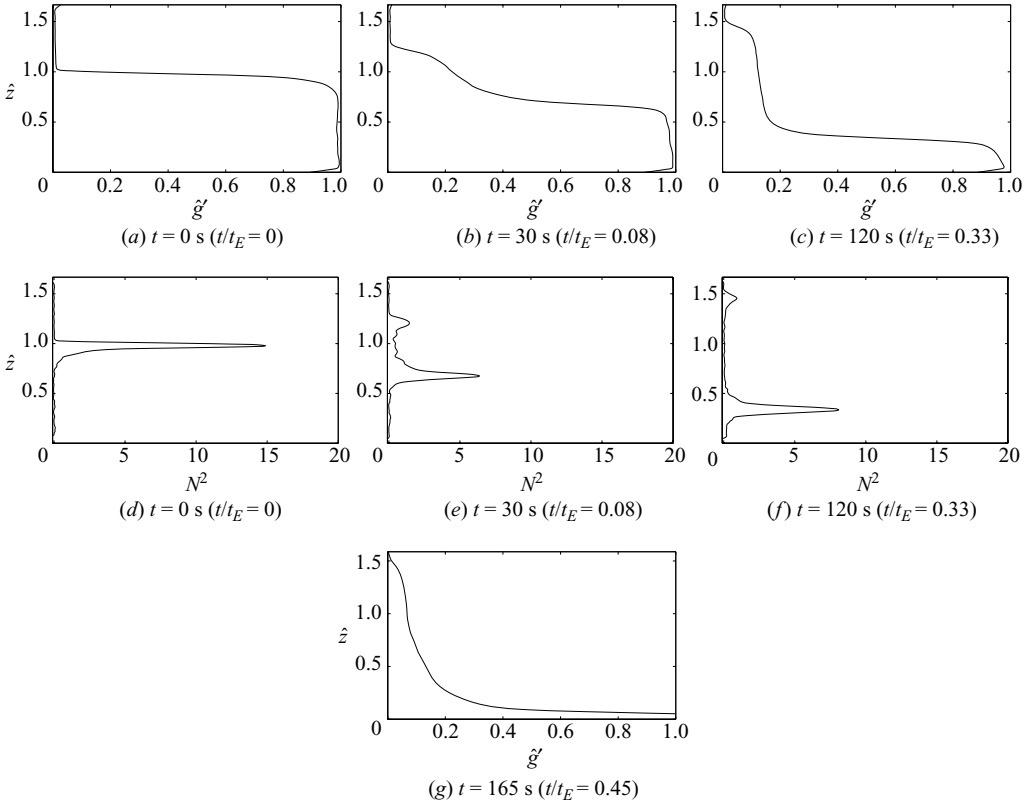


FIGURE 7. Reduced gravity profiles (*a–c, g*) and buoyancy frequency profiles (*d–f*) of the typical ‘displacement flow with interfacial mixing’ experiment shown in figure 6.

on the interface between the original two layers and penetrated the dense layer, developing as a turbulent fountain within this layer (figure 6). Turbulence at the impingement region entrained dense fluid from the lower layer which mixed with fluid at ambient density in the jet. The resulting mixture, of a density between that of the ambient and the original dense layer, spread laterally along the interface as an intrusion until reaching the walls of the box, thereby, forming an intermediate layer (figure 6*b*). The time scale for the formation of the intermediate layer was of the order of 5 s, i.e. small compared with t_E (table 1). The intermediate layer increased in depth as it was supplied both with fluid from the jet and fluid entrained from the dense layer. The three-layered nature of the developing stratification is clearly evident from the reduced gravity profiles (figures 7*b* and 7*c*) and from the twin peaks in the buoyancy frequency profiles (figures 7*e* and 7*f*). We note from figure 7(*c*) that mixing by the high-level inflow has caused a significant redistribution of buoyancy with approximately one third of the total buoyancy ($\mathcal{B} = S \int_0^H g' dz$) remaining, accumulated within the intermediate layer.

At later times, when the intermediate layer was sufficiently deep, the fountain collapsed back before reaching the lower interface and hence the mechanism for entrainment across the lower density interface was lost – in figure 6(*d*) the fountain impinges on the lower interface whereas in figure 6(*e*) the top of the fountain (labelled ‘A’) no longer reaches the lower interface signifying the end of the entrainment period. This behaviour is highlighted in the profiles shown in figure 7. Whilst the fountain

interacted with the lower layer, the intermediate layer was supplied with saline solution. This entrained flux reduced the density step between the lower two layers seen in figure 7(e) by a decrease in the peak buoyancy frequency (compare with figure 7d). Once the fountain/lower interface interaction ceased the intermediate layer was supplied solely with fluid at ambient density (and so diluted), thus the density step between the lower and intermediate layer increased – this is evident from the increased peak buoyancy frequency in figure 7(f) compared with figure 7(e).

Once the original dense layer had completely drained from the box, fluid from what was the ‘intermediate’ layer (and now the lowermost layer) began to drain out. This fluid loss reduced the rate of deepening, however, the layer slowly deepened to fill the box resulting in a weakly stratified interior (figure 7g).

The flow patterns observed in the unidirectional regimes (§§ 3.3.1 and 3.3.2) are dependent on the momentum flux of the high-level inflow. For a fixed a_T (and given stratification) the momentum flux of the inflow is controlled by the area a_B of the base opening. As a_B is increased, A^* increases and the volume flux out of the box increases (see (1.5)) and, thus, the momentum flux of the incoming jet of replacement fluid ($\propto Q^2/a_T$) increases. For sufficiently large values of a_B , the resulting high-Reynolds-number jet is able to fully penetrate the initial two-layer stratification resulting in turbulent mixing and the formation of a third layer. However, once a_B decreases below some critical value (§ 4), there is insufficient energy in the jet to penetrate the density interface in this way. Instead a depression is observed – turbulent scouring causes fluid to be lifted from the dense layer into the layer above although this scouring does not result in the formation of an intermediate layer. As a_B decreases still further, the velocities and shear associated with the inflow impingement are no longer large enough to ensure the development of a turbulent jet and turbulent scouring is no longer observed. The nature of the interfacial mixing and transition from pattern 1 to 2 is considered further in § 4.1.

3.4. Bidirectional flows

For top opening areas significantly smaller than base opening areas, typically for $a_T \lesssim (1/4)a_B$, unidirectional flow was no longer observed throughout the draining. Instead, fluid at ambient density was observed to enter the box through the base as an exchange flow established. The nature of the exchange observed was complex and varied during the drain. For all experiments in which exchange flows were observed, the exchange *ceased* once the original lower layer had fully drained and the flow then reverted to being unidirectional. By contrast, the exchange flow commenced either after some initial period of unidirectional flow or immediately at $t=0$. Typically, the exchange observed was initially weak (specifically the volume flux of fluid entering via the base was small relative to the volume flux through the top) and its strength increased as the original lower layer flushed. This exchange, however, was not continuous and was broken by intermittent periods of unidirectional outflow. As with the unidirectional regimes, the jet-like flow of replacement fluid through the top induced either weak (Δ) or vigorous (\blacktriangle) interfacial mixing.

3.4.1. \blacktriangle Pattern 3. Exchange flow with interfacial mixing

Figure 8 shows images from a typical experiment in which a mixing-like flow is established below the level of the original interface and there is vigorous interfacial mixing due to a jet-like inflow impinging from above. The corresponding dimensionless reduced gravity and buoyancy frequency profiles are shown in figure 9. In this regime, marked by the solid triangles (\blacktriangle) on the flow regime diagrams, interfacial mixing

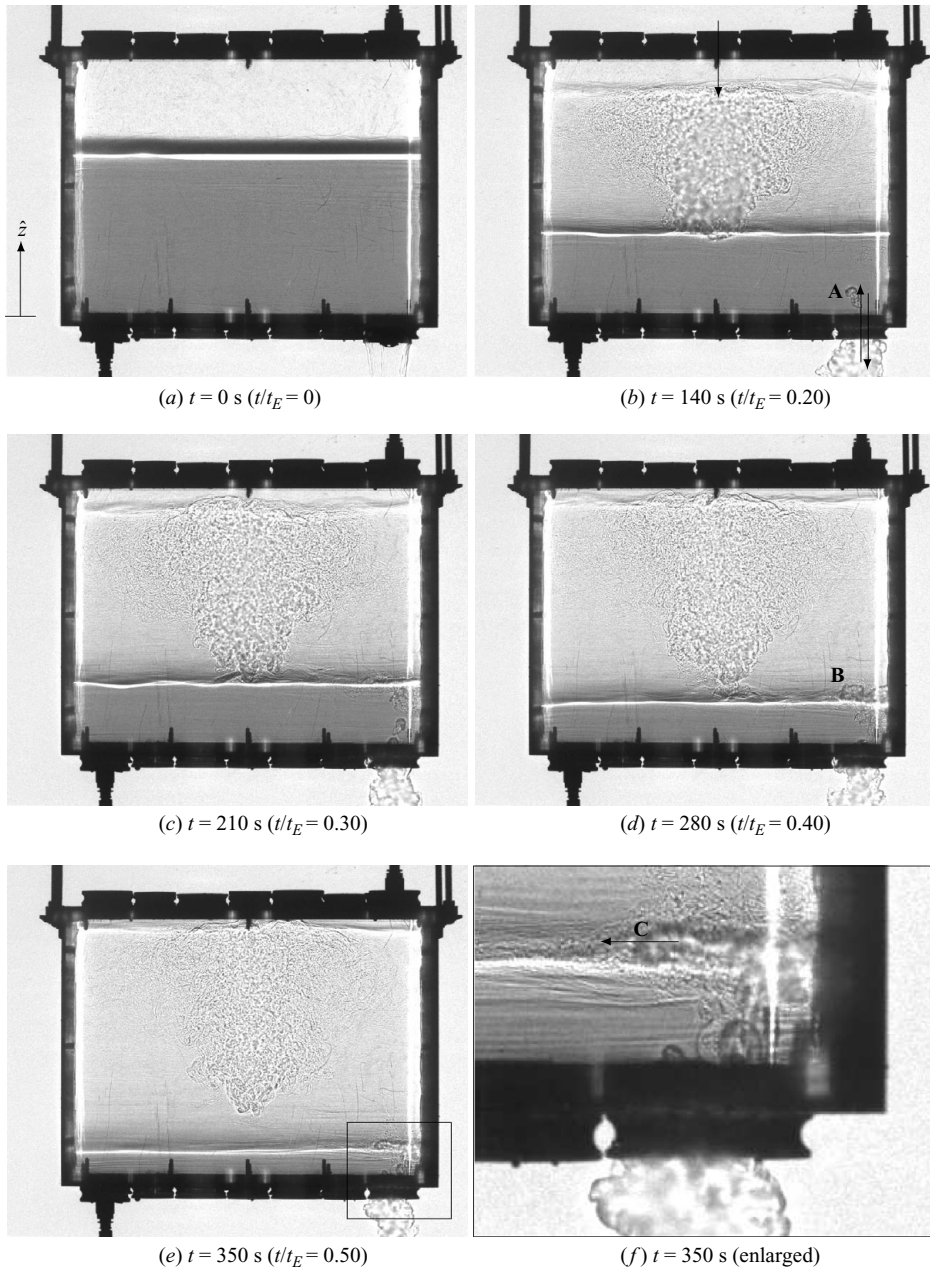


FIGURE 8. The bidirectional flow pattern ‘exchange flow with interfacial mixing’ (\blacktriangle in the flow regime diagrams). The arrows in (b) indicate the direction of flow, maintained for these initial conditions/geometry, through the openings. (a) The initial stratification. (b)–(e) As in figure 6 an intermediate layer formed during the transients. However, here a bidirectional flow is established at the base opening (seen in the exploded view, figure f).

driven by replacement fluid through the top again resulted in the formation of a third layer which deepened to fill the box. However, in contrast to the previous flow regimes, an exchange flow was observed at the base. This exchange can be seen during the initial transients on the shadowgraph (figure 8b to the right of the region marked

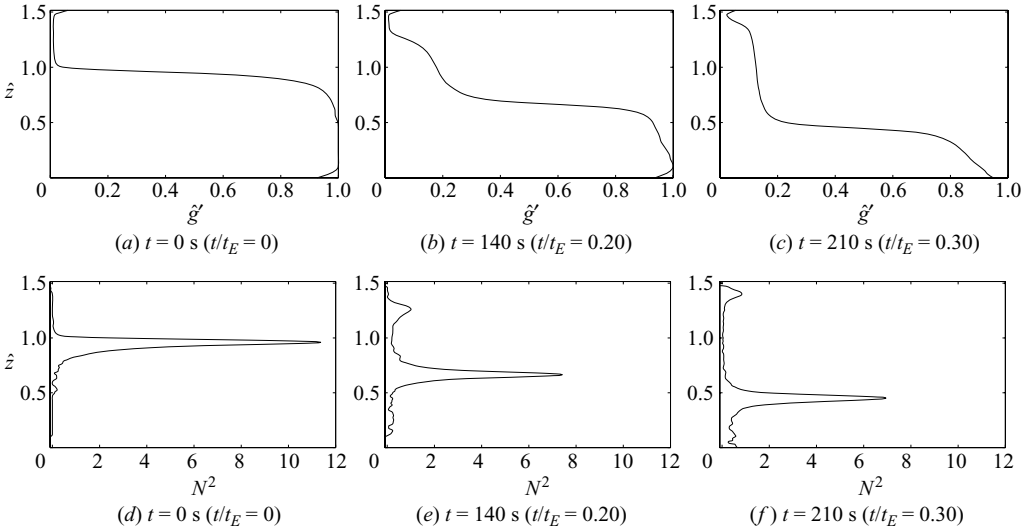


FIGURE 9. Reduced gravity profiles (a–c) and buoyancy frequency profiles (d–f) of the ‘exchange flow with interfacial mixing’ experiment shown in figure 8.

‘A’) and during the later transients in the exploded view (figure 8f). The onset of this exchange, shown as a sequence of images in figure 14, is considered in detail in §4.2.

Simultaneously, dense fluid drained out of and ambient fluid rose in through the base opening. Incoming fluid at ambient density ascended as a turbulent plume-/thermal-like flow and impinged on the density interface between the lower layer and layer at intermediate density (region immediately below ‘B’ in figure 8d). This impingement caused a weak entrainment of fluid from the intermediate layer into the dense layer below, reducing the net flux of volume into the intermediate layer and thereby restricting its rate of growth. Vigorous mixing due to the high-level inflow induced a three-layered stratification (figure 9c) and the resulting two interfaces persisted during the transients (figure 8b and 8c, and the two peaks in the buoyancy frequency profiles, figures 9e and 9f). We refer to this class of flows as ‘mixing flow with interfacial mixing’.

The lower layer gradually diluted over time (compare figures 9a–c) due to the introduction of fluid at ambient density via the base exchange. A weak stratification developed in the lower layer due to the rising plume/thermals driving a ‘filling box’-like process in this layer. Eventually, the dense layer completely drained from the box. At this time the exchange flow ceased.

As R decreased, for a fixed $\{\xi_0, \lambda_T\}$, the volume flow rate of the inflow through the base increased, thus reducing the net volume flux out of the lower dense layer. This resulted in an increase in the time taken to drain the original lower dense layer.

3.4.2. Δ Pattern 4. Exchange flow

Considering a box with a single top opening, reductions in R or ξ_0 (for a fixed λ_T) decrease the momentum flux of the inflow through the top opening until it is insufficient to cause vigorous interfacial mixing. A two-layer stratification then persists. Figure 10 shows images from a typical experiment in which interfacial mixing induced by inflow through the top was negligibly weak (so that an increase in the upper layer buoyancy could not be discerned with the density meter) and a strong exchange flow was established and maintained at the base (i.e. the inward volume flux across the

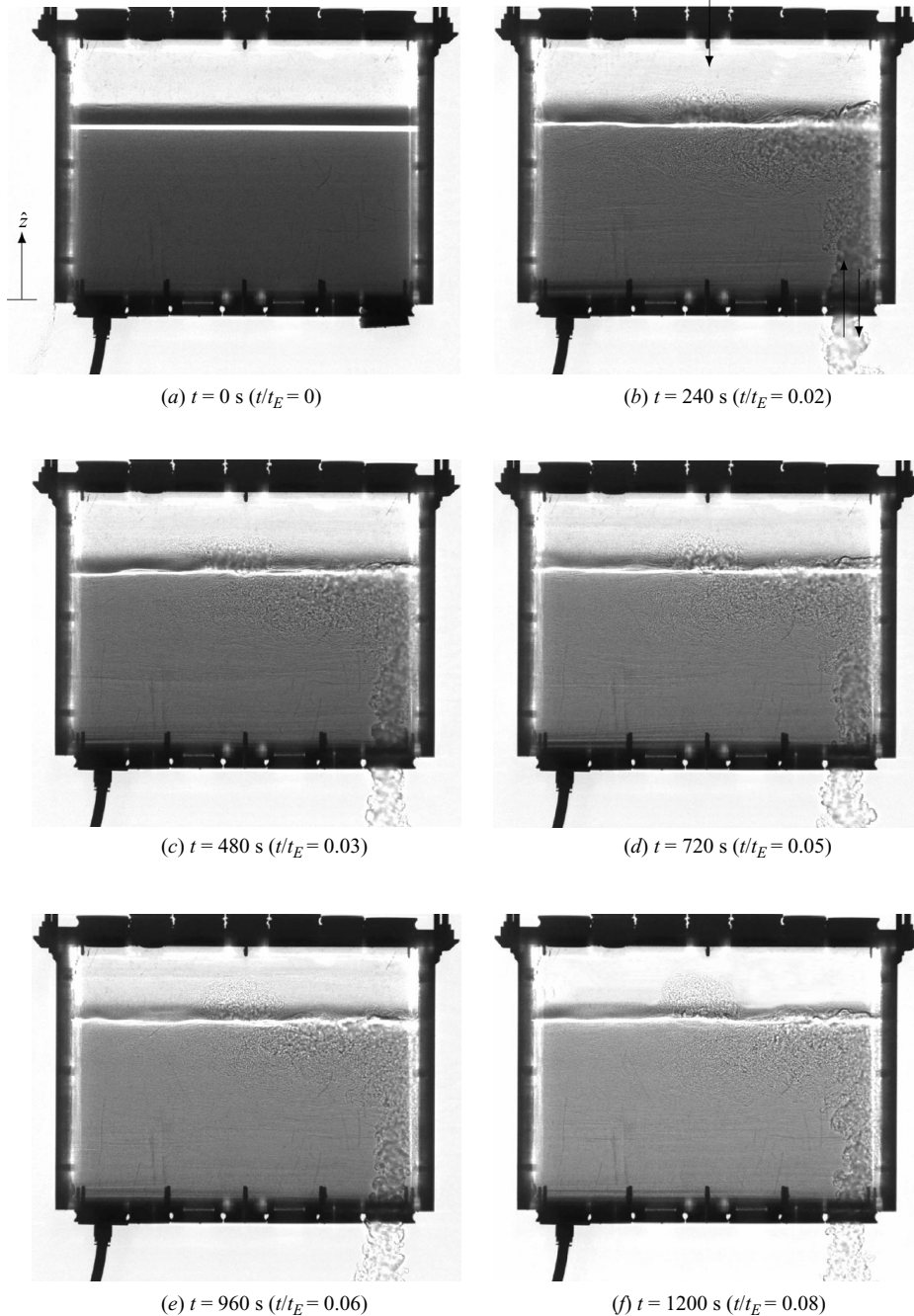


FIGURE 10. The bidirectional flow pattern ‘exchange flow’ (Δ in the flow regime diagrams). The arrows in (b) indicate the direction of flow maintained through the openings. (a) The initial stratification. (b)–(f) A two-layer stratification is maintained, however, in this regime the lower layer increases in depth, due to a net entrainment from the upper layer to the lower layer, and dilutes (visible by the lightening of the dyed layer).

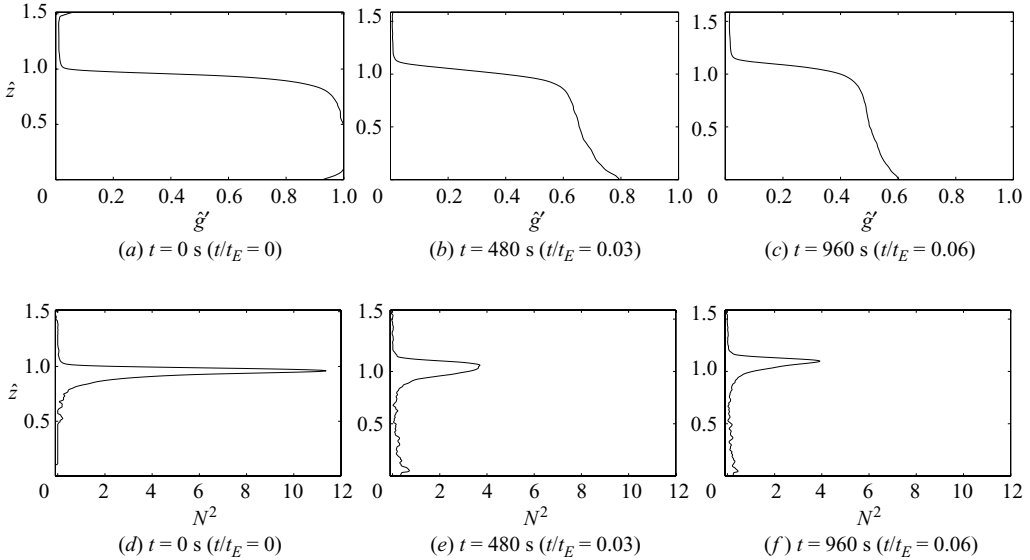


FIGURE 11. Reduced gravity profiles (a–c) and buoyancy frequency profiles (d–f) of the ‘exchange flow’ experiment shown in figure 10.

opening approximated the outward volume flux). Parameter values yielding this class of flow pattern, referred to as simply ‘exchange flow’, are indicated in the flow regime diagrams by the hollow triangles (Δ).

For all experiments conducted in this regime, the depth of the dense layer changed very slowly when compared to the other flow patterns identified. This suggests that the net volume flux out of this layer is relatively small and, thus, the volume fluxes entering and exiting the lower layer are almost equal. In this case, the exchange is referred to as ‘strong’; in contrast, exchanges in which the outward flux dominates (see figure 14) are described as ‘weak’. For very small R (typically $R \lesssim 0.01$) the lower dense layer was observed to increase in depth. The volume flux entrained from the upper layer into the lower layer, due to the impingement of the fluid rising through the base with the interface, then exceeds the volume flux through the top. Following the same argument one might reasonably expect that it is possible to establish a layer of approximately constant depth, at least for some period, when the rate of entrainment of ambient fluid into the lower layer (due to interfacial impingement from below) equals the volume flux through the top. Whilst a constant layer depth was not observed experimentally, flows were realized in which the rate of change of depth of the lower layer was very slow in comparison to the rate of dilution (figure 10).

For all exchange flows examined, the influx of fluid at ambient density through the base resulted in a decrease in the reduced gravity of the lower layer (compare figure 11a–c). The lower layer was not uniformly well mixed, rather a weak stratification established. This structure is attributed to buoyant fluid rising from the base and spreading horizontally on reaching the interface and thereby stratifying the intermediate layer by a process similar to that of the filling box (Baines & Turner 1969). The beginning of a horizontal intrusion, with front position labelled C and the direction of motion shown by the arrow, is clearly visible in the exploded image of figure 8(f).

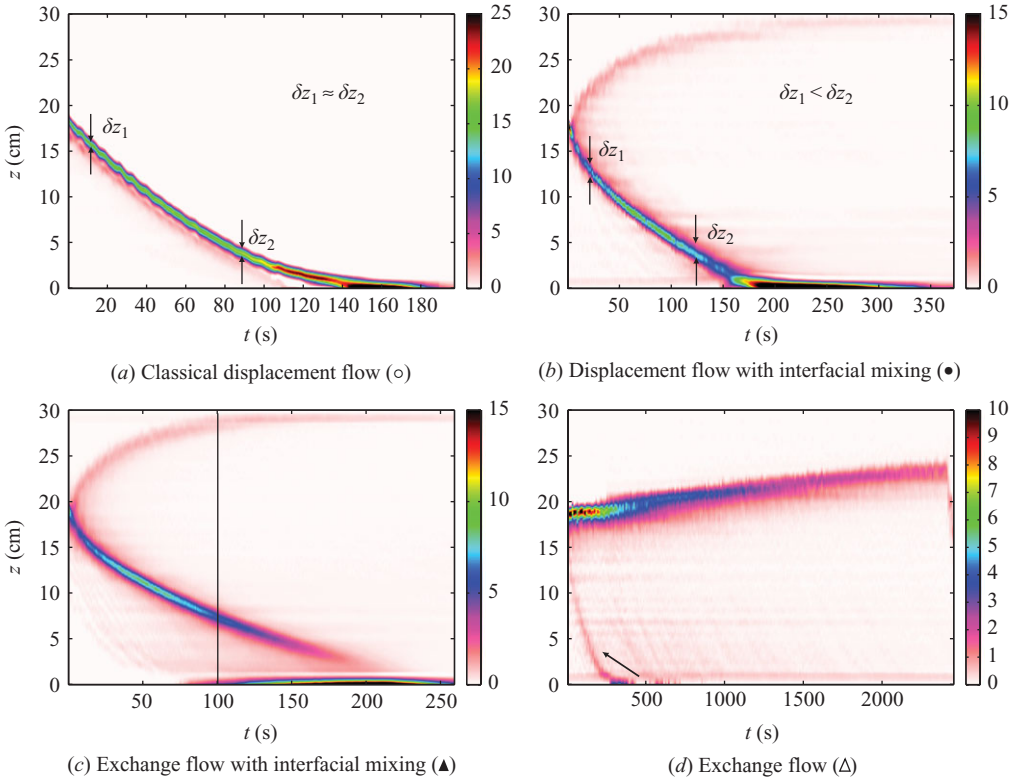


FIGURE 12. Time series of buoyancy frequency $N^2 = \partial \hat{g}' / \partial \hat{z}$ for the four flow patterns identified. Note that the horizontal axis and colour bars have different scales.

3.5. Summary

The key features of the four flow patterns identified and the distinctions between them are further revealed by comparing a time series of their respective buoyancy frequency profiles. The colour at an individual point on each time series in figure 12 represents, for an individual experiment, the value of the horizontally averaged buoyancy frequency ($N^2 = \partial \hat{g}' / \partial \hat{z}$) at the corresponding height and time. The colour map has been normalized for each experiment so that black corresponds to the maximum buoyancy frequency in that experiment. The data is presented in its raw dimensional form and highlights the lack of a single characteristic time scale.

For classical displacement flow (figure 12a), a single peak in the buoyancy frequency, shown by the green/yellow band, descends and corresponds to the single density interface between the two layers. Apart from a vertical transposition, the characteristics of the peak remain unaltered; with the width (see δz_1 and δz_2 on the figure) and the maximum value (shown by the colouring on the band) remaining constant with time. From these constant characteristics of the peak one may deduce that the inflowing replacement fluid is not able to significantly smear or alter the density step across the interface.

For displacement flow with interfacial mixing (figure 12b), two peaks are present for the majority of the transients. Unlike classical displacement flow, the width of the lower peak (blue/green band) increases in time ($\delta z_2 > \delta z_1$) due to the upward flux of buoyancy induced by the jet-like high-level inflow/entraining fountain. The rising

weaker upper peak (faint pink band) also increases in width and the peak value decreases. The N^2 value that the upper peak attains appears to reduce noticeably when the fountain stops impinging on the lower interface (figure 6e and in figure 12b for $t \gtrsim 120$ s) and, thus, when the intermediate layer is thereafter diluted solely with fluid at ambient density. For $t \gtrsim 200$ s no strong gradients remain.

For exchange flow with interfacial mixing (figure 12c), the time series is initially qualitatively similar to that of figure 12(b) ($t \lesssim 100$ s). This similarity is as a consequence of a weak inflow through the base (see e.g. figure 8b). However, at later times the influence of the inflow through the base on the stratification becomes more significant due, in part, to the increasing strength of the base-level inflow relative to the outflow and to the decreasing volume of the lower layer. This is visible (to the right of the vertical line on figure 12c) by a continued widening of the peak and marked decrease in the peak's maximum value. Furthermore, in contrast to figure 12(b), the region of strong gradient in the density profile is unable to reach the base of the box due to the action of the exchange flow.

For exchange flow (figure 12d), a single significant peak in the buoyancy frequency is observed and ascends. A second weaker peak is also visible, indicated by an arrow in the figure, with these density gradients established as the base-level inflow stratifies the lowermost layer in a series of 'descending fronts' (cf. Baines & Turner 1969). The magnitude of the significant peak decreases in time as a consequence of the reduction in the density step across the interface due to base-level inflow diluting the lower layer, and owing to the turbulence associated with the top-level inflow smearing the interface. Note that, in contrast to the flow in figure 12(c), here the exchange flow plays a significant role throughout the draining.

4. Transitions between flow patterns

We now develop scalings for the transitions between flow patterns. In §4.1 the transition between flow patterns with and without interfacial mixing is considered and in §4.2 the transition between unidirectional and bidirectional flow.

4.1. Mixing across the interface

The transition from classical displacement flow (flow pattern 1, ○) to displacement flow with interfacial mixing (flow pattern 2, ●) occurred, for example, on decreasing R (for fixed ξ_0 and λ_T) when the momentum flux of the inflowing jet (M_T) was sufficiently large to disrupt the otherwise stable density interface and turbulently entrain fluid from the lower layer to establish an intermediate layer. Assuming a uniform velocity profile across the top opening

$$M_T(0) = \frac{Q_T(0)^2}{a_T} = \frac{A^{*2} g'_0 h_0}{a_T} = \frac{2c_T^2}{1 + \frac{a_T^2 c_T^2}{a_B^2 c_B^2}} a_T g'_0 h_0 = \frac{2c_T^2}{1 + \frac{c_T^2}{c_B^2} R^2} \lambda_T^2 \xi_0^3 g'_0 H^3, \quad (4.1)$$

where $M_T(0) \equiv M_T(t=0)$ and $Q_T(0) \equiv Q_T(t=0)$ are the initial momentum and volume fluxes through the top, respectively. Thus, for a fixed $\{R, \xi_0, \lambda_T\}$, $M_T(0)$ increases as g'_0 increases. However, this increase in the strength of the jet and, thus, its ability to induce mixing is counteracted by the increased stability of the interface resulting from the increased density contrast (see (4.3)).

Turbulent entrainment across a density interface is often characterized by an interfacial Froude number $Fr_i = w_i / (b_i \Delta g')^{1/2}$, where w and b are the centreline vertical velocity and radius of the inflowing jet, respectively, and $\Delta g'$ is the reduced

gravity step across the interface; the subscript ‘ i ’ denoting the value of the variable at the interface. For convenience, we henceforth drop the subscript ‘ i ’ on Fr . A number of researchers have examined turbulent mixing at, and entrainment across, density interfaces. Linden (1973) examined vortex rings impinging on density interfaces and proposed that such a ring could be considered an approximation to a turbulent eddy. His experimental results supported a theoretical argument that the volume flux Q^* turbulently entrained across an interface scales as $Q^*/(b^2w) \sim Fr^3$. Baines (1975) and Kumagai (1984) both performed experiments investigating the entrainment across density interfaces due to impinging plumes and jets. Baines (1975) found that $Q^*/(b^2w) \propto Fr^3$, while Kumagai (1984) proposed the empirical formula $Q^*/(b^2w) = Fr^3/(1 + 3.1Fr^2 + 1.8Fr^3)$ which reduces to $Q^*/(b^2w) = Fr^3$ for $Fr \ll 1$ and $Q^*/(b^2w) = 0.56$ for $Fr \gg 1$. Lin & Linden (2005a) examined entrainment across density interfaces due to turbulent fountains and, for the range of interfacial Froude numbers examined ($Fr > 0.9$) gave $Q^*/(b^2w) = 0.65 \pm 0.17$.

Modelling the inflow through the top opening as a fully developed self-similar axisymmetric turbulent jet, the classic scalings (Fischer *et al.* 1979) give the jet velocity and radius at the density interface, at time $t = 0$, as

$$w_i(t = 0) = w_0 = \alpha_{jet} M_T(0)^{1/2} (H - h_0)^{-1} \quad \text{and} \quad b_i(t = 0) = b_0 = \beta_{jet} (H - h_0), \quad (4.2)$$

where the empirical constants $\alpha_{jet} = 7.0 \pm 0.1$ and $\beta_{jet} = 0.107 \pm 0.003$. With these scalings the initial interfacial Froude number associated with flow in through the top opening, $Fr_T(0) = w_0/(b_0 g'_0)^{1/2}$, can be expressed purely geometrically, i.e. independently of g'_0 :

$$Fr_T(0) = 2^{1/2} \frac{\alpha_{jet}}{\beta_{jet}^{1/2}} \frac{\lambda_T}{R} \left(\frac{1}{c_B^2} + \frac{1}{c_T^2 R^2} \right)^{-1/2} \left(\frac{1}{\xi_0} - 1 \right)^{-3/2}. \quad (4.3)$$

On examination of (4.3) one may deduce that, consistent with our experimental results, the initial interfacial Froude number, and thus the initial vigour of interfacial mixing, increases as either R is decreased, λ_T is increased or ξ_0 is increased (holding the other two parameters constant in each case). The scaling for Fr_T in (4.3) is developed on the assumption that the origin of the jet is coincident with the plane of the opening at $z = H$. Hence, this is expected to provide a useful estimate provided $H - h_0 \gg \sqrt{a_T}$, i.e. the vertical extent of the jet is large compared with its source scale. Including an origin correction for the jet $\hat{z}_v = \lambda_T/(\beta_{jet}\pi^{1/2})$, estimated geometrically by tracing the jet back to a point source, gives

$$Fr_T(0) = 2^{1/2} \frac{\alpha_{jet}}{\beta_{jet}^{1/2}} \frac{\lambda_T}{R} \left(\frac{1}{c_B^2} + \frac{1}{c_T^2 R^2} \right)^{-1/2} \left(\frac{1}{\xi_0} - 1 + \hat{z}_v \right)^{-3/2}. \quad (4.4)$$

For a given geometry, the momentum flux of the inflowing jet is determined by the total buoyancy \mathcal{B} contained within the box ($M_T(t) \sim \int_0^H g'(z, t) dz$). Buoyancy is lost continuously as dense fluid drains out through the base and the maximum value of the momentum flux (and, hence, the maximum ability of the inflow to cause mixing) occurs at $t = 0$. Thus, $Fr_T(0)$ characterizes the maximum level of mixing due to the inflow and we expect a critical initial interfacial Froude number, $Fr_{T,c}$ say, above which interfacial mixing is significant, i.e. as seen for flow pattern 2 or 3 (● or ▲, respectively), to mark a transition from flow pattern 1 to 2. In other words, for $Fr_T(0) = w_0/(b_0 g'_0)^{1/2} = Fr_{T,c} = \text{constant}$ to define a boundary between flow patterns with and without interfacial mixing. Figure 13 plots $w_0/(g'_0 h_0)^{1/2} = Fr_{T,c} (b_0/h_0)^{1/2}$ for $Fr_{T,c} = 0.67$ together with our experimental data.

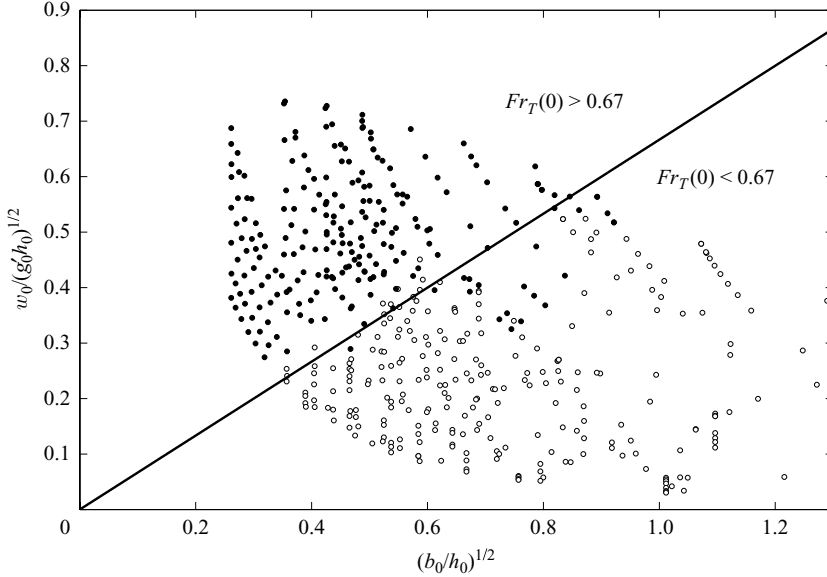


FIGURE 13. The dimensionless initial centreline jet velocity at the interface $w_0/(g'_0 h_0)^{1/2}$ plotted against the dimensionless jet width at the interface $(b_0/h_0)^{1/2}$. ○ No interfacial mixing observed. ● Significant interfacial mixing observed. The solid line shows the critical initial interfacial Froude number $Fr_{T,c} = 0.67$.

It is clear that the line $Fr_{T,c} = 0.67$ defines well the boundary between the regimes. We attribute the limited scatter across the boundary primarily to disturbances induced on removal of the plugs (§2) from the holes in the box. The solid line in the flow regime diagrams shows the contour $Fr_T(0) = Fr_{T,c} = 0.67$. We have only drawn this contour for the portion of the parameter space where unidirectional flow is observed (○ and ●). For bidirectional flow (4.4) is not valid as the volume flux through the top $Q_T(0) \neq A^* \sqrt{g'_0 h_0}$, thus $M_T(0) \neq (A^{*2} g'_0 h_0)/a_T$. Again, it can be seen (figure 3) that $Fr_T(0) = Fr_{T,c} = 0.67$ separates well the experimentally observed regimes. Thus, if $Fr_T(0) \lesssim 0.67$ we expect interfacial mixing to be insignificant, otherwise we expect a break down of the initial two-layer stratification and the formation of an intermediate layer.

For an initially 'full' box $h_0 = H$ ($\xi_0 = 1$) and using (3.4), (4.4) reduces to

$$Fr_T(0) = 2^{1/2} \frac{\alpha_{jet} \beta_{jet} \pi^{3/4}}{R \lambda_T^{1/2}} \left(\frac{1}{c_B^2} + \frac{1}{c_T^2 R^2} \right)^{-1/2} = \frac{A^* \alpha_{jet} \beta_{jet} \pi^{3/4}}{H^2 \lambda_T^{5/2}}. \quad (4.5)$$

Thus to ensure a classical displacement flow actually requires

$$\frac{A^*}{H^2} < \frac{Fr_{T,c} \lambda_T^{5/2}}{\alpha_{jet} \beta_{jet} \pi^{3/2}} \approx 0.377 \lambda_T^{5/2}, \quad (4.6)$$

rather than any combination of $a_T > 0$ and $a_B > 0$. For the two sets of measurements presented by Linden *et al.* (1990), we estimate

- (i) $\lambda_T = \frac{\sqrt{52.7}}{25}$ and $A^*/H^2 \approx \frac{18.4}{25^2} = 0.029 \not< 0.377 \lambda_T^{5/2} \approx 0.017$;
- (ii) $\lambda_T = \frac{\sqrt{28.9}}{25}$ and $A^*/H^2 \approx \frac{4.3}{25^2} = 0.007 < 0.377 \lambda_T^{5/2} \approx 0.008$.

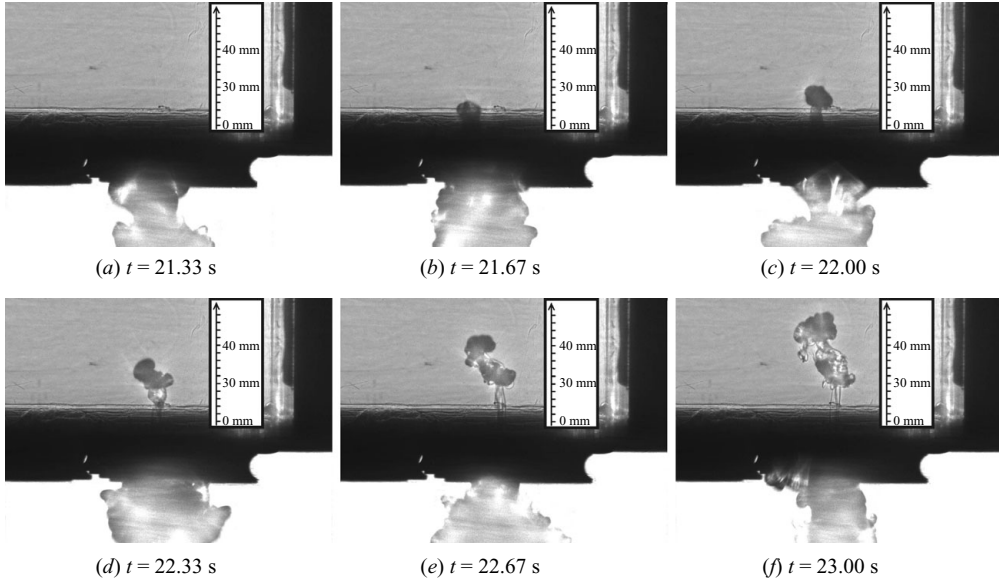


FIGURE 14. Shadowgraph images of a typical first ‘burst event’ at the base opening. The plume-like outflow and the thermal-like nature of the inflow are shown. Images correspond to flow pattern 3 in table 1. (a) Solely outflow. (b)–(f) Combined inflow and outflow.

4.2. The transition to bidirectional flow

The development of a number of flows began as unidirectional flow but during the later transients non-sustained bursts of inflow were observed at the base opening, which rose against the dominant outflow – these intermittent bursts being distinct from the accepted notion of an exchange in which both inflow and outflow occur continuously across an opening. Shadowgraph images of a typical ‘burst event’ are shown in figure 14. The flow through the base opening was predominantly outflow. The inflow took the form of rising thermal-like pulses of fluid. Following the first ‘burst’, the base opening flow typically reverted to unidirectional outflow. Subsequent bursts became increasingly energetic and advected larger volumes of buoyant inflow which rose and created wave-like disturbances on the original density interface. Based on our observations of the thermal-like nature of the inflow, which signalled a departure from a continuous unidirectional flow, we now develop a simple model for isolating the range of emptying-box starting conditions $\{R, \xi_0, \lambda_T\}$ which we expect will lead to this non-unidirectional behaviour. Our aim is to formulate a constraint on the starting conditions that enable a buoyant thermal to rise into the box via the base opening, i.e. against the mean downward flow. Figure 15 depicts the basic situation considered and the nomenclature adopted.

Suppose a volume of fluid at ambient density enters the box via the base opening and rises as a thermal. From Scorer (1957), the vertical velocity ω of the thermal at a height z is, to a first approximation,

$$\omega(z) = c(g'_B V_B)^{1/2} (z + z_v)^{-1}, \quad (4.7)$$

where g'_B and V_B are the reduced gravity and volume of the thermal at the plane of the base opening $z = 0$, respectively, c (≈ 1.2) is an empirical constant and z_v the distance to a virtual origin below the thermal. We assume a spherical thermal so that $V_B = \frac{4}{3}\pi(D_B/2)^3$, where D_B denotes the diameter of the thermal at the plane of the

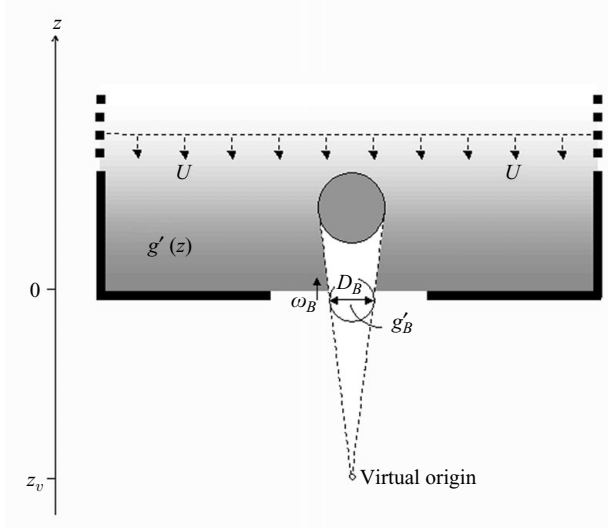


FIGURE 15. A schematic of the emptying box in the region of the base opening illustrating the incoming thermal (shown as a circular disk) in the plane of the base opening and at the height where its rise speed equals the speed of the downward flowing environment.

opening. To estimate z_v we appeal to the fact that the radius of a thermal increases linearly with height $r = \beta z$, where $\beta \approx 1/4$ from Scorer (1957), hence $z_v = -D_B/(2\beta)$.

For conditions close to the transition between unidirectional and bidirectional flows, the inward volume flux through the base opening is very weak (figure 14) and the mean vertical velocity in the box with instantaneous stratification $g'(z, t)$ is approximated by

$$U = \begin{cases} -\frac{Q_B}{a_B} & \text{for } z \ll \sqrt{a_B}, \\ -\frac{Q_B}{S} & \text{for } z \gg \sqrt{a_B}, \end{cases} \quad (4.8a)$$

where

$$Q_B \approx A^* \sqrt{\int_0^H g'(z, t) dz} = \sqrt{2} a_T \left(\frac{1}{c_T^2} + \frac{R^2}{c_B^2} \right)^{-1/2} \sqrt{\int_0^H g'(z, t) dz}. \quad (4.8b)$$

The ratio of velocities $|U(z=0)/\omega(z=0)| = |U_B/\omega_B|$ at the base opening enables us to establish whether a thermal is able to rise ($|U_B/\omega_B| < 1$) or is advected out of the box ($|U_B/\omega_B| > 1$). From (4.7) and (4.8),

$$\left| \frac{U_B}{\omega_B} \right| = \left(\frac{3}{2\pi} \right)^{1/2} \frac{1}{c\beta} \frac{A^*}{a_B} \sqrt{\frac{\int_0^H g' dz}{D_B g'_B}} = \left(\frac{3}{\pi} \right)^{1/2} \frac{R}{c\beta} \left(\frac{1}{c_T^2} + \frac{R^2}{c_B^2} \right)^{-1/2} \sqrt{\frac{\int_0^H g' dz}{D_B g'_B}}. \quad (4.9)$$

Denoting the diameter of the thermal at the plane of the opening as a constant fraction δ ($0 < \delta \leq 1$) of the base opening diameter (i.e. $D_B = 2\delta\sqrt{a_B/\pi}$), (4.9)

reduces to

$$\left| \frac{U_B}{\omega_B} \right| = \frac{3^{1/2}}{2^{1/2}\pi^{1/4}} \frac{R}{c\beta\delta^{1/2}} \left(\frac{1}{c_T^2} + \frac{R^2}{c_B^2} \right)^{-1/2} \sqrt{\frac{\int_0^H g' dz}{a_B^{1/2} g'_B}}. \quad (4.10)$$

In terms of the outward fluxes of volume (Q_B), momentum (M_B) and buoyancy (F_B) at the base opening (4.10) reduces to

$$\left| \frac{U_B}{\omega_B} \right| = \frac{3^{1/2}}{2\pi^{1/4}} \frac{1}{c\beta\delta^{1/2}} Fr_B, \quad Fr_B = \frac{M_B^{5/4}}{Q_B F_B^{1/2}}, \quad (4.11)$$

where $F_B = Q_B g'_B$ and we have assumed that the outward velocity profile across the base opening is uniform so that $M_B = Q_B^2/a_B$. The dimensionless quantity Fr_B is a Froude number expressed in terms of fluxes through the base opening. Thus, we expect

$$Fr_B = \frac{M_B^{5/4}}{Q_B F_B^{1/2}} = 2^{1/2} \left(\frac{1}{c_B^2} + \frac{1}{c_T^2 R^2} \right)^{-1/2} \sqrt{\frac{\int_0^H g' dz}{a_B^{1/2} g'_B}} = \text{constant} \quad (4.12)$$

to characterize the flow through the base opening and provide the scaling for the transition. For the two-layer stratification considered herein the initial value of Fr_B ($= Fr_B(0)$) reduces to

$$Fr_B(0) = \frac{A^*}{a_B} \sqrt{\frac{h_0}{a_B^{1/2}}} = 2^{1/2} \lambda_T^{-1/2} R^{1/4} \left(\frac{1}{c_B^2} + \frac{1}{c_T^2 R^2} \right)^{-1/2}. \quad (4.13)$$

Note that, as we are considering flow through the base, it is convenient to express $Fr_B(0)$ in terms of $\lambda_B = \sqrt{a_B/h_0}$ (see § 3.1):

$$Fr_B(0) = 2^{1/2} \lambda_B^{-1/2} \left(\frac{1}{c_B^2} + \frac{1}{c_T^2 R^2} \right)^{-1/2}. \quad (4.14)$$

Figure 16 shows $2^{1/2} \lambda_B^{-1/2}$ plotted against $((1/c_B^2) + (1/c_T^2 R^2))^{1/2}$ for the suite of experiments we performed and thus the position of each point is indicative of the initial value of Fr_B . The contour along which $Fr_B(0) = 0.33$ (shown by the solid line) cleanly separates the unidirectional (\circ , \bullet) and bidirectional (\triangle , \blacktriangle) flow patterns. This suggests that knowledge of the *initial* value of Fr_B , and thus of the initial fluxes, is sufficient to predict a transition between unidirectional and bidirectional flows – a transition which may occur either initially or at some later stage during the transients. For $Fr_B(0) > 0.33$ we expect the flow through the base opening to remain unidirectional throughout the transients, i.e. from $t = 0$. For $Fr_B(0) < 0.33$ a bidirectional flow is expected although not necessarily from $t = 0$. The region between the curves (figure 16) $Fr_{B,c} = 0.2 < Fr_B(0) < 0.33$ confining those experiments which exhibited unidirectional flow during the initial transients and later developed an exchange at the base. This exchange was observed only while the original dense layer remained in the box. However, once this layer had fully drained, the exchange ceased and the flow reverted to unidirectional flow. The boundary $Fr_B = 0.2$ was found by considering the evolution of Fr_B , using (4.12), for five experiments and estimating its value at the onset of exchange. We see that the flow pattern 4 experiments, for which an exchange was observed from $t = 0$, satisfy the condition $Fr_B(0) < 0.2$ (i.e. they lie below the dotted line in figure 16) giving confidence in this bound.

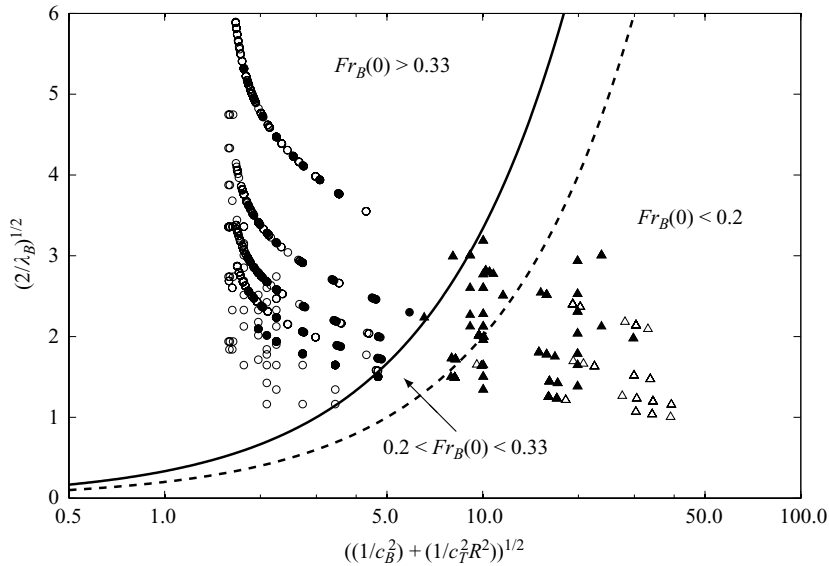


FIGURE 16. Log-linear plot of $(2/\lambda_B)^{1/2}$ against $((1/c_B^2) + (1/c_T^2 R^2))^{1/2}$. \circ and \bullet unidirectional flows, \triangle and \blacktriangle bidirectional flows. The solid line is the contour $Fr_B(0) = 0.33$ and separates well the unidirectional and bidirectional flows. The dashed line is the contour $Fr_B(0) = Fr_{B,c} = 0.2$. For $Fr_B(0) < 0.2$ bidirectional flow was observed at the base opening from $t = 0$.

The scatter in figure 16 is attributed to the fact that (4.13) assumes a sharp two-layer stratification, whereas, in the experiments some smearing of the initial density stratification was unavoidable (see e.g. figure 5a).

4.3. Discussion

Whilst we developed the scaling for transition, Fr_B , by considering the velocity of a rising thermal in a mean downward flow, the dependence on Fr_B may be deduced from a number of alternative perspectives, thereby highlighting the robustness of this scaling.

To begin with, note that Fr_B is proportional to the ratio of volume fluxes driven by displacement and mixing flows, i.e. $Fr_B \propto Q_d/Q_m$. We recall from §1 that $Q_m (\propto a_B^{5/4} \sqrt{g_B})$ is the volume flux expected if a classical mixing flow were established (i.e. a balanced exchange across the base opening and zero volume flux through the top) and $Q_d (= A^* \sqrt{\int_0^H g' dz})$ is the volume flux expected if a classical displacement flow were established (i.e. unidirectional flow through base and top openings and an absence of interfacial mixing). Thus, $Fr_B \ll 1$ implies that exchange flow will yield a higher volume flux out of the box, whereas $Fr_B \gg 1$ implies displacement flow will result in a higher volume flux.

Alternatively, one would expect the behaviour of a high-Reynolds-number unidirectional flow at the base opening to be determined purely by the relative fluxes of momentum, volume and buoyancy as the outflow is plume-like. A Richardson number $\Gamma = 2^{-7/2} \alpha_p^{-1} \pi^{1/2} Q_B^2 F_B M_B^{-5/2} \propto 1/Fr_B^2$ (where α_p is the plume entrainment coefficient) is used to classify the source conditions of plumes (see e.g. Morton 1959). Thus, we might have anticipated the onset of an exchange flow when the outflowing plume was sufficiently lazy (i.e. for $\Gamma \gg 1$). The critical Froude number $Fr_{B,c} = 0.2$ corresponds to $\Gamma = \Gamma_c \approx 70$. This is in accordance with the work of Hunt & Kaye

(2001) who, on investigating lazy plumes using a simple nozzle design, were unable to reach such a large value of Γ without observing a bidirectional flow at the plume source.

A third physical argument for the transition to bidirectional flow is based on the position at $z = z_n$ of the neutral pressure level (NPL) – namely, the level at which the pressures inside and outside the box are identical. Determining the NPL is relatively straightforward (Appendix) and for a box containing an arbitrary stratification $g'(z, t)$, z_n satisfies the implicit expression

$$\frac{c_T^2}{c_B^2} R^2 = \frac{\int_0^{z_n} g'(z, t) dz}{\int_{z_n}^H g'(z, t) dz}. \quad (4.15)$$

If $a_T \equiv 0$ (and $a_B > 0$) the NPL is coincident with the plane of the base opening. If $a_T > 0$, the NPL is above the base opening. Our observations suggest that small fluctuations in the exterior environment may trigger fingers of ambient density fluid to grow and enter through the base opening, see the region denoted ‘A’ in figure 8(b). For $z < z_n$ internal pressures exceed those at the same horizontal level in the exterior. Conversely, for $z > z_n$ external pressures exceed those in the interior. Thus, we hypothesize that if these fingers grow to reach the NPL before being advected back out of the box, they will continue to grow and remain in the box. In other words, if the NPL is sufficiently close to the base of the box, these fluctuations will result in an inward flux of ambient fluid across the base opening in addition to the outward flux of dense fluid – i.e. exchange flow. The closer the NPL to the base, the greater the number of fingers expected to grow to the NPL and so the stronger the inflow. We expect exchange when the NPL is within a characteristic length scale ($\propto \sqrt{a_B}$) of the base opening. For the two-layer initial stratification considered herein, this pressure-based approach leads to a dependence on the same parameter Fr_B as the velocity-based approach of §4.2 as from (4.15), a NPL at $z_n = z_c$ (i.e. at a critical distance above the base opening so exchange can occur) requires

$$\frac{z_c}{\sqrt{a_B}} = \frac{Fr_B(0)^2}{2c_B^2}. \quad (4.16)$$

Taking $Fr_B(0) = 0.33$ and $c_B = 0.6$ we have $z_c/\sqrt{a_B} = 0.15$, implying that exchange may be expected if $0 \leq z_n \lesssim 0.15\sqrt{a_B}$. For our experiments this gives $z_c = 0.4 \text{ cm} \lesssim 0.15\sqrt{a_B} \lesssim 0.9 \text{ cm}$, however we were unable to accurately determine the critical NPL directly. The equivalent of figure 16 in terms of the height $z = z_c$ of the NPL is shown in figure 18 (Appendix).

The NPL approach, in particular, shows the importance of the stratification on the likelihood of exchange. By redistributing the buoyancy within the box the NPL may be raised or lowered (see (4.15)), thus inhibiting or encouraging exchange to occur, respectively. Thus, the interfacial mixing prevalent in flow patterns 2 and 3 actually works to inhibit exchange as, by raising dense fluid, the NPL is elevated further away from the base opening. We may therefore expect that the onset of exchange would occur at a larger value of $Fr_B(0)$ if the momentum of the inflow through the top opening were diffused such that interfacial mixing was inhibited. In the context of a naturally ventilated building containing warm air this could be achieved by diffusers (e.g. mesh, gauze or grills) placed over the low-level opening.

5. Conclusions

We have investigated the dynamics of emptying boxes, i.e. the draining of buoyant fluid from a box into a quiescent environment of uniform and constant density. Focus has been on a box (height H), with openings in the top (area a_T) and base (area a_B) faces, whose interior is initially stably stratified in two homogenous layers – a layer at ambient density separated by a sharp horizontal interface from a buoyant layer. Our attention has been restricted to high-Reynolds-number flows and density differences that are small compared with the density of the ambient. Additionally, we have concerned ourselves only with boxes of cross-sectional areas $S \gg \{a_T, a_B\}$. This constraint is met in the majority of building ventilation flows, a potential area of application of this work, as open window/vent areas are typically less than 5% of the floor area.

A programme of laboratory experiments reveals that one of a range of four possible flow patterns may be established, which result in a bulk vertical motion in the box, depending on the initial depth of the buoyant layer relative to the box height ($\xi_0 = h_0/H$) and the box geometry, as characterized by the opening area ratio $R = a_T/a_B$ and $\lambda_T = \sqrt{a_T}/h_0$. The density of the buoyant layer relative to the ambient density only influenced the time scale for the development of a given flow and not the flow pattern realized.

We categorized the different patterns observed depending on whether (a) the direction of the flow at the base opening, through which buoyant fluid drained out, was unidirectional or bidirectional, and whether (b) replacement fluid at ambient density, which flowed into the box through the top opening, resulted in vigorous interfacial mixing.

Previous research indicated that either displacement flow, which occurs in the absence of mixing at the interface by the replacement fluid and maintains a unidirectional flow through openings, or mixing flow, whose bidirectional flow through the base opening results in vigorous mixing and an interior maintained at an approximately uniform density, are the only patterns possible. Notably, for the former, a two-layer stratified interior was thought to persist, provided openings were made in both top and base, and that the behaviour could be adequately described solely in terms of an effective opening area (A^*) relative to the square of the box height (H), and the box cross-sectional area S .

We have shown that the aforementioned displacement and mixing flows represent idealized limiting cases of no-mixing and complete-mixing by the replacement fluid, respectively; that these flows occupy only a fraction of the $\{R, \xi_0, \lambda_T\}$ parameter space; and that, in general, the dynamics of the emptying process are far more complicated with turbulent inflow of fluid (through either top or base openings) yielding varying degrees of mixing and stratification breakdown.

Our scalings and experimental data indicate that the flow from an emptying box can be classified in terms of two Froude numbers. The first, Fr_T based on the dynamics of the replacement fluid through the top opening and the interfacial density contrast. The second, Fr_B based on the dynamics of the flow through the base opening. As a consequence we were able to deduce that the top opening controls the extent of interfacial mixing and the base opening controls the direction of flow.

If one considers the flow of replacement fluid through the top of the box then interfacial mixing significantly alters the stratification from its initial form if $Fr_T \gtrsim 0.66$. In this case, vigorous turbulent mixing results in the development of a layer of intermediate density which deepens to fill the box, i.e. whilst the total buoyancy reduces with time the box actually fills rather than empties. In the context

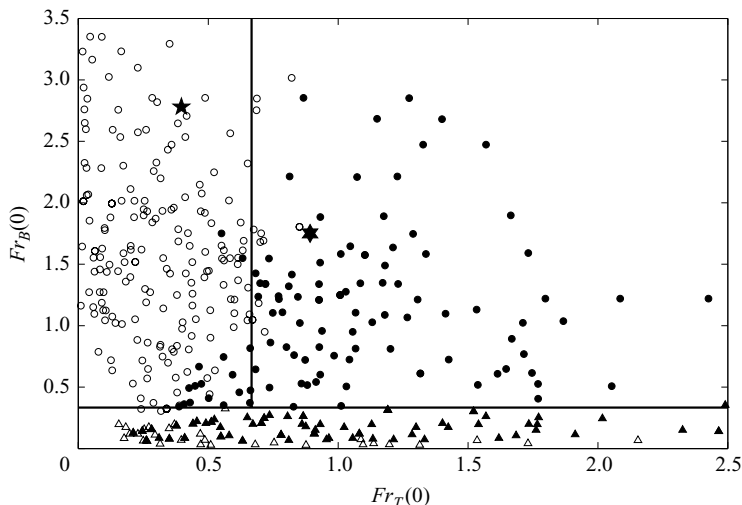


FIGURE 17. Plot of $Fr_B(0)$ versus $Fr_T(0)$ highlighting how the two Froude numbers are sufficient to classify the four flow patterns. The vertical line is $Fr_T(0) = 0.67$ and the horizontal line is $Fr_B(0) = 0.33$. The stars (★ and ★) show the experiments performed by Linden *et al.* (1990) ($a_T = 52.7 \text{ cm}^2$, $a_B = 23.8 \text{ cm}^2$ and $a_T = 28.9 \text{ cm}^2$, $a_B = 5.1 \text{ cm}^2$, respectively and $h_0 = H = 25 \text{ cm}$).

of purging heat from a building at night, this may lead to unexpected thermal conditions on the following day and come as a surprise to the architect or ventilation engineer who may reasonably have expected warm air to rise and empty from the building.

If one considers the direction of flow through the base of the box then unidirectional flow is maintained provided $Fr_B \gtrsim 0.2$. For $Fr_B \lesssim 0.2$ replacement fluid flows into the box through both the top and base openings. As Fr_B may be expressed as a ratio of volume flow rates, we may reinterpret conditions for bidirectional flow as those for which the volume flow rate that would be driven through the base opening if (classical) mixing flow were assumed is at least a factor of five greater than that which would be driven by (classical) displacement flow through the same area of openings.

Figure 17 shows the flow regime diagram replotted as $Fr_B(0)$ against $Fr_T(0)$. This clearly highlights how the pair of Froude numbers $\{Fr_T(0), Fr_B(0)\}$ at the onset of the flow can be used to classify the transient emptying-box flows considered herein into one of the four flow patterns (○, ●, ▲, △). It also exposes a limitation of this classification, namely, that we are unable to state Fr_T for the bidirectional flows (i.e. if $Fr_B(0) < 0.33$ and $a_T > 0$) as the volume flow rate through the top opening is currently undetermined. Also shown (★ and ★) are the respective Froude numbers for the experiments performed by Linden *et al.* (1990) in their investigations of classical displacement flows. We note that, for one of their experiments (★), interfacial mixing may have been significant. This may explain the variation in their data from the classical displacement flow theory they developed. Our scalings show that in fact true classical displacement flows only occur if $A^*/H^2 \lesssim 0.4(a_T/H^2)^{5/4}$ (from (4.7)).

Whilst we have considered only an initial two-layered stratification we expect the same basic range of flow patterns and our general classification to hold for other stable initial stratifications. Furthermore, if openings were instead made in the vertical walls of the box (as per the location of windows and doors in typical buildings) or multiple openings made (as per an underfloor air distribution (UFAD)

system, Lin & Linden 2005*b*) one would expect a similar pattern of flows to develop albeit with different constant values for the Froude numbers at the transitions. Whilst we expect the same basic range of flow patterns to be realized, further work targeting the effect of multiple openings in the base and top would be informative.

A primary application of the results described is to the natural, or passive, ventilation of buildings. As a consequence of the range of flow patterns we have identified and notably the ‘displacement flow with interfacial mixing’ we are able to deflect the criticism levelled at the use of fresh and salt water solutions to model natural ventilation flows at small scale.

Mathematical models of flow patterns 2–4 (as described in §§3.3.2, 3.4.1 and 3.4.2) are currently being developed by the authors. Additionally, the work presented herein is being extended to include effects of mixing by the inflow on the steady stratification established by a continuous buoyancy input to mirror the emptying–filling box (conducted in the absence of mixing by replacement fluid) work of Linden *et al.* (1990). This coupled with the possibility of simultaneous exchange and unidirectional flows through multiple openings at base level offers challenging avenues for future research.

The authors gratefully acknowledge Arup and the EPSRC for their financial support of this project. We would also like to thank the BP Advanced Energy Programme in Buildings at Imperial for their financial support.

Appendix. Transition to bidirectional flow based on the neutral pressure level (NPL)

In order to predict the transition between the unidirectional and bidirectional flow patterns, the NPL (at $z = z_n(t)$) is considered. A straightforward analysis following Linden *et al.* (1990) yields

$$\frac{c_T^2}{c_B^2} R^2 = \frac{\int_0^{z_n(t)} g'(z, t) dz}{\int_{z_n(t)}^H g'(z, t) dz}. \quad (\text{A } 1)$$

To lower the NPL towards the base opening (i.e. for $z_n \rightarrow 0$) requires $a_T \rightarrow 0$, as expected.

For the initial two-layer density stratification considered herein,

$$\frac{c_T^2}{c_B^2} R^2 + 1 = -\frac{h_0}{(z_n - h_0)} \quad \text{or} \quad z_n = h_0 \left(1 + \frac{c_B^2}{c_T^2} R^{-2} \right)^{-1}. \quad (\text{A } 2)$$

Note that, as expected, $z_n \rightarrow 0$ in the limits $a_T \rightarrow 0$ or $a_B \rightarrow \infty$ (i.e. $R \rightarrow 0$); and $z_n \rightarrow h_0$ in the limits $a_B \rightarrow 0$ or $a_T \rightarrow \infty$ (i.e. $R \rightarrow \infty$).

It is expected that the transition between unidirectional and bidirectional flows will occur at a critical value of z_n , for example, when $z_n = z_c$. As we expect the scale of the base opening to be key in governing the onset to exchange, we propose that $z_c \propto \sqrt{a_B}$ or

$$\frac{z_c}{\sqrt{a_B}} \propto \frac{R^{1/2}}{\lambda_T} \left(1 + \frac{c_B^2}{c_T^2} \frac{1}{R^2} \right)^{-1} = \frac{Fr_B(0)^2}{2c_B^2}. \quad (\text{A } 3)$$

Figure 18 shows $1/\lambda_T = (2/\lambda_B)^{1/2}$ plotted against $R^{-1/2}((1 + c_B^2/c_T^2)(1/R^2))$ and thus represents the initial value of $z_n/\sqrt{a_B}$ for the experiments performed. From the

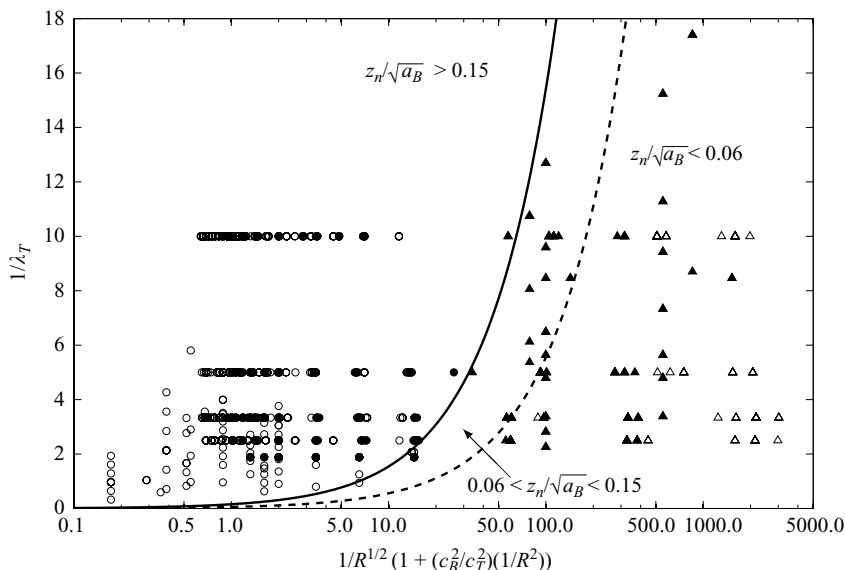


FIGURE 18. Log-linear plot of $1/\lambda_T$ against $1/R^{1/2} (1 + (c_B^2/c_T^2)(1/R^2))$. \circ and \bullet unidirectional flow, \triangle and \blacktriangle bidirectional flow. The solid line is the contour $z_n/\sqrt{a_B} = 0.15$ (equivalent to $Fr_B(0) = 0.33$) and separates well the unidirectional and bidirectional flows. The dashed line is the contour $z_n/\sqrt{a_B} = 0.06$ (equivalent to $Fr_B(0) = 0.2$). For $z_n/\sqrt{a_B} < 0.06$ bidirectional flow is observed at the base opening from $t = 0$.

figure we can see that an initial NPL of $z_n \approx 0.15\sqrt{a_B}$ divides the flow patterns into unidirectional and bidirectional regimes.

REFERENCES

- BAINES, W. D. 1975 Entrainment by a plume or jet at a density interface. *J. Fluid Mech.* **68** (2), 309–320.
- BAINES, W. D. & TURNER, J. S. 1969 Turbulent buoyant convection from a source in a confined region. *J. Fluid Mech.* **37**, 51–80.
- BATCHELOR, G. K. 1967 *An Introduction to Fluid Mechanics*. Cambridge University Press, ISBN 0–521–66396–2.
- CENEDESE, C. & DALZIEL, S. B. 1998 Concentration and depth field determined by the light transmitted through a dyed solution. In *Proceedings of the eighth Intl Symp. on Flow Visualization* (ed. G. M. Carlomagno & I. Grant), ISBN 0953 3991 09, paper 061.
- COFFEY, C. J. & HUNT, G. R. 2007 Ventilation effectiveness measures based on heat removal. Part 2. Application to natural ventilation flows. *Build. Environ.* **42** (6), 2249–2262.
- DALZIEL, S. B. 1993 Rayleigh–Taylor instability: experiments with image analysis. *Dyn. Atmos. Oceans* **20**, 127–153.
- EPSTEIN, M. 1988 Buoyancy-driven exchange flow through small openings in horizontal partitions. *J. Heat Transfer* **110**, 885–893.
- FISCHER, H. B., LIST, E. J., KOH, R. C. Y., IMBERGER, J. & BROOKS, N. H. 1979 *Mixing in Inland and Coastal Waters*. Academic Press, ISBN 0–12–258150–4.
- HACKER, J., LINDEN, P. F. & DALZIEL, S. B. 1996 Mixing in lock-release gravity currents. *Dyn. Atmos. Oceans* **24**, 183–195.
- HUNT, G. R. & KAYE, N. G. 2001 Virtual origin correction for lazy turbulent plumes. *J. Fluid Mech.* **435**, 377–396.
- HUNT, G. R. & LINDEN, P. F. 2001 Steady-state flows in an enclosure ventilated by buoyancy forces assisted by wind. *J. Fluid Mech.* **426**, 355–386.

- KUMAGAI, M. 1984 Turbulent buoyant convection from a source in a confined two-layered region. *J. Fluid Mech.* **147**, 105–131.
- LIN, Y. J. P. & LINDEN, P. F. 2005a The entrainment due to a turbulent fountain at a density interface. *J. Fluid Mech.* **542**, 25–52.
- LIN, Y. J. P. & LINDEN, P. F. 2005b A model for an under floor air distribution system. *Energy Build.* **37** (4), 399–409.
- LINDEN, P. 1973 The interaction of a vortex ring with a sharp density interface: a model for turbulent entrainment. *J. Fluid Mech.* **60**, 467–480.
- LINDEN, P. F., LANE-SERFF, G. F. & SMEED, D. A. 1990 Emptying filling boxes: the fluid mechanics of natural ventilation. *J. Fluid Mech.* **212**, 309–335.
- MORTON, B. R. 1959 Forced plumes. *J. Fluid Mech.* **5**, 151–163.
- SCORER, R. S. 1957 Experiments on convection of isolated masses of buoyant fluid. *J. Fluid Mech.* **2** (6), 538–594.
- TORRICELLI, E. 1643 *De Motu Gravium Naturaliter Accelerato*. Firenze .
- TURNER, J. S. 1973 *Buoyancy Effects in Fluids*. Cambridge University Press.